ELSEVIER

Journal of Nuclear Materials 244 (1997) 101–130

journal of nuclear materials

RACLETTE: a model for evaluating the thermal response of plasma facing components to slow high power plasma transients. Part II: Analysis of ITER plasma facing components

Gianfranco Federici, A. René Raffray *

ITER Garching JWS, c / o Max-Planck-Institut für Plasmaphysik, Boltzmannstr 2, D-85748 Garching, Germany

Received 10 May 1996; accepted 16 September 1996

Abstract

The transient thermal model RACLETTE (acronym of Rate Analysis Code for pLasma Energy Transfer Transient Evaluation) described in part I of this paper is applied here to analyse the heat transfer and erosion effects of various slow (100 ms–10 s) high power energy transients on the actively cooled plasma facing components (PFCs) of the International Thermonuclear Experimental Reactor (ITER). These have a strong bearing on the PFC design and need careful analysis. The relevant parameters affecting the heat transfer during the plasma excursions are established. The temperature variation with time and space is evaluated together with the extent of vaporisation and melting (the latter only for metals) for the different candidate armour materials considered for the design (i.e., Be for the primary first wall, Be and CFCs for the limiter, Be, W, and CFCs for the divertor plates) and including for certain cases low-density vapour shielding effects. The critical heat flux, the change of the coolant parameters and the possible severe degradation of the coolant heat removal capability that could result under certain conditions during these transients, for example for the limiter, are also evaluated. Based on the results, the design implications on the heat removal performance and erosion damage of the various ITER PFCs are critically discussed and some recommendations are made for the selection of the most adequate protection materials and optimum armour thickness.

1. Introduction

The in-vessel components of the International Thermonuclear Experimental Reactor (ITER), namely the primary first wall, the limiter, the baffle and the divertor, will be subject during normal operation to high heat loads generated by particles (C–X neutrals, ions and electrons) impact, as well as electromagnetic radiation. Highest heat loads are anticipated onto the surfaces of the divertor and, during plasma start-up and shutdown phases, onto the limiter. Various types of off-normal conditions such as disruptions and edge localised modes are foreseen, that will substantially increase the heat flux for very short times on these components and will cause significant armour erosion due to vaporisation and partial loss of melt in metals and appreciable electrodynamic stresses in the plasma facing components (PFCs) and surrounding structures. In addition, at some locations, the PFCs must withstand a certain number of so called 'slow' high-power plasma thermal transients, whose duration is anticipated to be much longer than that of disruptions, and of the same order of the

* Corresponding author. Tel.: +49-89 3299 4406; fax: +49-89 3299 4163; e-mail: raffrar@sat.ipp-garching.mpg.de.

PII S0022-3115(96)00681-2

characteristic thermal diffusivity of the actively cooled component itself. These have bearing on the design of the PFCs and need careful analysis. An example of this class of events include transients expected periodically onto the so called 'vertical target' in the divertor system, near the separatrix–strike points, because of high-recycling transients burning through the gas target regime [1,2]. They will last up to a few seconds and increase the surface heat-flux from the peak design value of ~ 5 MW/m^2 to a range of 10–30 MW/m^2. High-power transient loads are also expected on the primary first-wall, limiter and upper part of the baffle modules during accidental plasma contact during burn, e.g., resulting from plasma vertical displacement events (VDEs). During this transient events, the plasma would typically deposit ≤ 60 MJ/m^2 in times ranging between 100 ms and 1 s.

Very fast ($\sim$ 1–10 ms) high energy density (10–100 MJ/m^2) plasma transients associated with disruptions result in armour material evaporation and melting, but have little or no thermal effects on the actively cooled heat-sink substrate and coolant. In contrast, 'slow' plasma transients not only produce substantial erosion of the armour through vaporisation and melting but lead to large heat flux propagation from the armour to the heat sink and to the coolant, potentially resulting in very high temperatures and stress at the interface between the armour and the heat sink and in drastic changes in the coolant heat removal capability.

The primary objective of this study is to analyse the thermal response of ITER PFCs subject to this category of high transient heat loads and to identify the relevant parameters affecting or governing the heat transfer process during these transients for the various plasma protection materials presently contemplated by the design. The analysis focuses on the limiter and divertor since these are the components under the more demanding steady state heat flux level in addition to the 'slow' high power transient events. All the calculations presented here have been carried out using the model RACLETTE (acronym of Rate Analysis Code for pLasma Energy Transfer Transient Evaluation) which is described in Part I of this paper [3]. The model provides for the solution of the heat conduction problem across a duplex structure (armour/heat sink) and includes evaporation, radiation, melting of the armour material and convective heat removal at the coolant side. Vapour shielding effects can be and have been included for some of the cases presented. The model provides a flexible design tool and is particularly suitable for fast parametric analyses of PFC behaviour under 'slow' high power transients as discussed by the authors in Ref. [3].

An extension of the original model has been made and is described in this paper to conveniently analyse some special cases anticipated to be particularly critical for the limiter, primary first wall (PFW) and baffle modules. For these cases, depending on the energy deposition time and the coverage, the heat flux to the coolant from a transient plasma energy deposition can be quite high, and two-phase flow conditions can be reached resulting in drastic changes in the heat transfer and in the pressure drop that could lead to dryout.

The organisation of the paper is as follows. First, the design layout of the ITER PFCs is briefly described, with emphasis on those components subject to the more demanding heat loads as well as to slow high power plasma transients (i.e., limiter and divertor). The procedure adopted to calculate the critical heat flux and the pressure drop for single-phase and subcooled boiling flow is then presented, followed by a discussion of the design parameters, heat loads and material properties of interest for the analysis. Next, the results of the various analyses performed are presented, first for the first wall components, with a focus on the limiter, and then for the divertor. Finally, key findings are summarised with emphasis on the implications of the results on the performance and lifetime of the various PFCs analysed and recommendations are made for the selection of the armour materials and thicknesses to be used.

2. Design highlights of PFCs in ITER

Fig. 1 taken from Ref. [4] shows a vertical cross-section of the ITER device. The blanket/first wall (FW) system [5] consists of ~ 2 m $\times$ 1 m FW-shield modules attached to a semi-permanent back plate by bolts which can withstand the tension loads during disruptions. A welded attachment scheme is also under consideration as an alternative. From the poloidal cross-section of Fig. 1, the lowest modules on the inboard and outboard are the baffle modules whose function is to attenuate the neutral flux from the divertor to the main chamber by a factor of at least 10^{-4}, the lowest two but one modules on the outboard are the start-up and shut-down limiter modules, and all the remaining modules are primary first wall (PFW) modules. The cooling water is supplied to the modules by inlet and outlet branch pipes connected to poloidally running inlet and outlet manifolds. The branch pipes can be cut and welded from inside the manifold by in-manifold remote handling equipment to enable module replacement if needed. Maintenance of the blanket modules will be performed by an in-vessel transporter inserted through the mid plane port [6]. Both the structural and shielding materials are SS 316 LN. The heat sink material is a Cu alloy. The cooling pipes are SS 316 LN in the primary first wall. For the limiter and the baffle first wall, Cu alloy tubes are used possibly with a thin SS liner or with Ni–Cr plating. All the FW and limiter modules are clad with Be. In the case of the limiter, carbon–fibre-composites (CFCs) are also considered as an alternative for the armour.

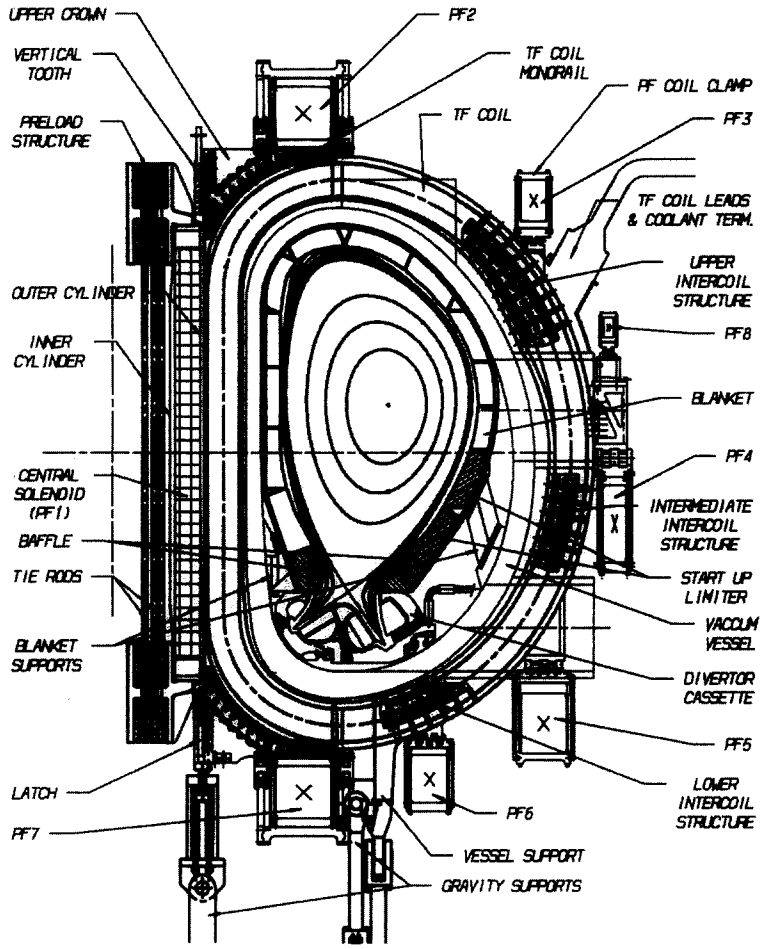

Fig. 1. Layout of plasma facing components in ITER [4].

In ITER, a single null poloidal divertor with active pumping located at the bottom of the device will provide for power and particle exhaust [4]. The divertor is designed to enhance the radiation losses in the divertor and control the location of the radiating region by confining the recycling of neutral impurities and hydrogen to the divertor chamber [2,7,8]. The reference design employs a so-called 'vertical target' concept which has the advantage that the plasma provides a tight seal for the neutrals together with an increase in the 'wetted' area (i.e., the area where the power conducted in the scrape-off layer is concentrated) due to the inclination of the divertor plates.

The divertor assembly consists of 60 cassettes which provide the interface to the ITER machine and to the in-vessel remote handling tools [9]. High heat flux components (HHFCs) are mounted onto these cassettes outside the vessel (in a hot cell), allowing periodical refurbishment of the cassettes and thus minimising radioactive waste. This solution also provides flexibility in the choice of the divertor geometry and thus permits adjustment to new divertor physics developments. Presently, three candidate materials are considered for protection of the divertor plasma facing components: beryllium, tungsten and CFCs attached to a Cu-alloy heat sink.

Typical concepts of the primary first wall, limiter and baffle, and divertor duplex structure configurations are shown in Fig. 2. They consist of a coolant tube embedded in a Cu-alloy heat sink structure on top of which is bonded the armour material. To minimise manufacturing complexity and enhance performance predictability, regular cooling tubes are preferred for the PFW, baffle and limiter. However, for the divertor vertical target region, cooling tubes with swirl tape inserts are considered because of the more demanding heat load requirements.

While the primary first wall uses tubes of stainless-steel, the limiter and baffle use Cu alloy tubes because of the higher heat flux requirements preferably with a thin SS insert (0.1–0.2 mm) or Ni–Cr plating inside the coolant tube to avoid Cu interfacing with water. This avoids the uncertainty associated with Cu/H_2O corrosion and erosion possibly leading to high

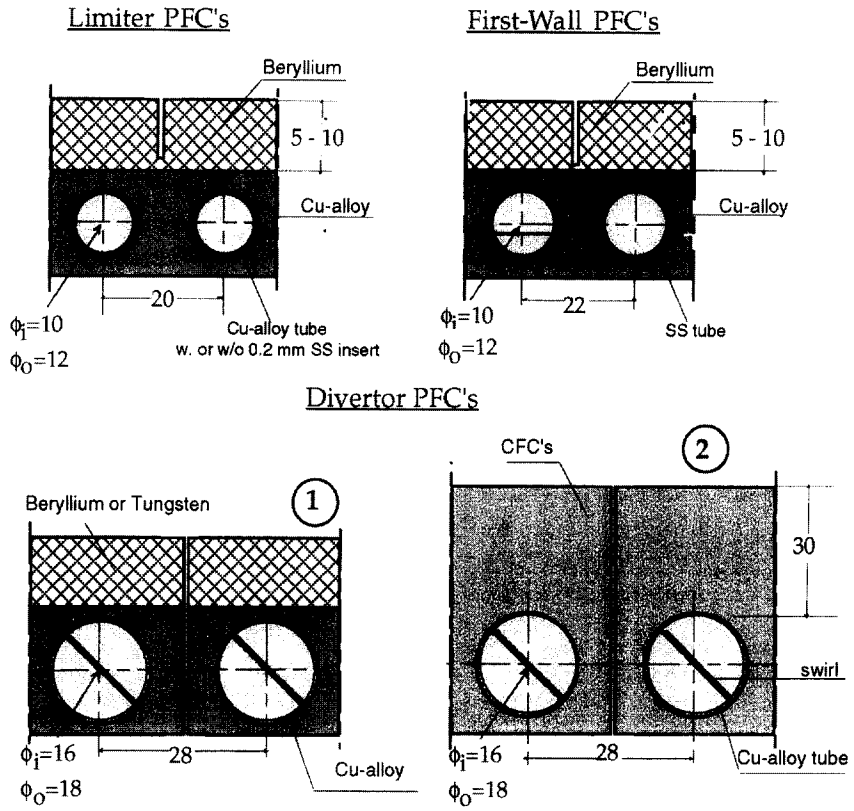

Fig. 2. Example configurations of actively cooled PFCs proposed for ITER (all dimensions in mm).

level of activated products in the coolant, and is the basis for eliminating the safety-based need for an intermediate heat exchanger in the cooling system.

3. Basis of the analysis

3.1. Model and code highlights

The RACLETTE model is used here to evaluate the response of the PFCs due to slow high-power plasma transients. For a given plasma heat flux history and coverage on a PFC structure, and a set of inlet coolant parameters, the model calculates the temperature distribution during the transient, melted and vaporised thicknesses, and the coolant properties at the outlet section. Further developments are under way to include other subsequent effects produced in materials such as stress and displacements. The model and the calculation procedure including the ranges of applicability have been thoroughly described in Part I of this paper [3]. It entails the solution of a heat conduction problem with two moving boundaries at the plasma-side (the liquid surface and the melt-solid interface) with a surface boundary condition determined by the dynamic of evaporation and a convective-heat transfer condition at the coolant side which allows for coolant flow in single-phase, and partially and fully-developed subcooled boiling regimes. Vapour shielding effects as calculated from a simplified model [7] have been included for some of the calculations. In this model, a low-density vapour shield develops in front of the target as the surface temperature increase due to vaporisation of material from the surface, leading to a conversion of some of the incident power to radiation, a fraction of which continues to fall on the plate, reaching about 25% of the incident power. It should be noted that, in contrast to the case of disruption erosion, the power levels here are lower by over 3 orders of magnitude, i.e., the 'vapour shield' from impurity contamination has much lower density and may therefore be expected to be optically thin. While several cases with vapour shielding are discussed in this paper, the JET experiment [10] indicated that vapour shield formation may not be as effective in reducing the power, and that significant melt layer loss may occur.

In order to better understand the consequences of high heat fluxes to the coolant following a plasma transient, a RACLETTE sister code was developed to calculate the coolant pressure drop and mass velocity as a function of the coolant

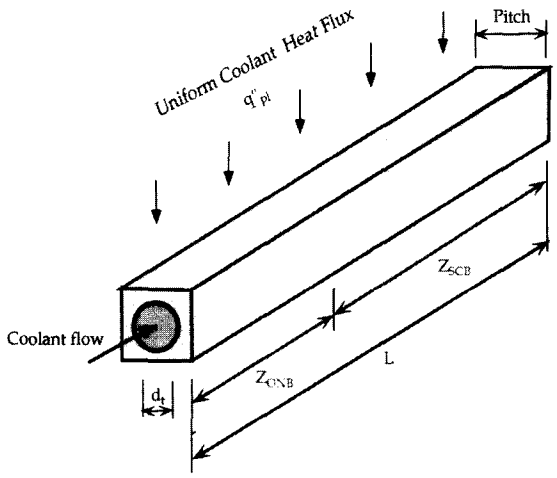

Fig. 3. Pressure drop flow model for uniform one-sided heat flux to the coolant.

heat flux. The results could then be used as input in RACLETTE thereby coupling the surface processes and heat transfer to the thermal-hydraulic conditions. In addition, the capability to estimate the critical heat flux based on the coolant conditions at each time step was added to RACLETTE.

3.2. Extension to the original model

3.2.1. Pressure drop model

The pressure drop along a coolant channel is calculated based on the flow regime. Thus, the flow characteristic along the channel must first be determined. The model used is illustrated in Fig. 3 which shows a coolant channel of length L under uniform one-sided heating. If the heat flux is low enough the flow through the whole length of the channel will be in single phase. As the heat flux is increased the flow will eventually consist of a single phase part up to a length of tube corresponding to the onset of nucleate boiling, Z_{ONB}, and of a subcooled boiling part over Z_{SCB}. Z_{ONB} is determined from the flow conditions and the heat flux to the coolant.

The Bergles and Rohsenow model shown in Eq. (1) is used to determine the onset of nucleate boiling (ONB) [11],

$$(T_w - T_{sat})_{ONB} = 0.556\left(\frac{q''_{ONB}}{1082\,P^{1.156}}\right)^{0.463P^{0.0234}}, \tag{1}$$

where $(T_w - T_{sat})_{ONB}$, the difference between the wall temperature and the water saturation temperature at ONB, is in K, the coolant pressure, P, in bars and the heat flux, q'', in W/m^2.

The wall temperature at ONB, $T_{w,ONB}$, can also be determined based on the heat flux, the water temperature and the single phase heat transfer coefficient:

$$T_{w,ONB} = \frac{f_{2D}\,q''_{PL}}{h} + T_{b,ONB}, \tag{2}$$

where f_{2D} is a factor to account for 2D effects ($\sim y_p/0.5\pi d_t$ [3], where y_p is the pitch, d_t is the tube diameter), q''_{PL} is the incident heat flux, $T_{b,ONB}$ is the water bulk temperature at ONB, and h is the convective heat transfer coefficient, estimated from the Dittus–Boelter correlation

$$Nu = \frac{hd_t}{k_f} = 0.023\,Re_f^{0.8}\,Pr_f^{0.33}. \tag{3}$$

Here, k_f is the water thermal conductivity, Re_f is the Reynolds number and Pr_f is the Prandtl number.

$T_{b,ONB}$ is calculated from the inlet temperature, water mass velocity and heat flux over a tube length Z_{ONB},

$$T_{b,ONB} = T_{b,IN} + \frac{q''_{PL}\,y_p Z_{ONB}}{GC_p\pi\left(d_t^2/4\right)}, \tag{4}$$

where G and C_p are the coolant mass velocity and specific heat, respectively. Z_{ONB} can be solved for by equating the

expression for $T_{w,ONB}$ from Eq. (1) to that from Eq. (2) in which Eq. (4) is substituted for $T_{b,ONB}$, and by re-arranging the final expression

$$Z_{ONB} = \frac{0.556\left(q''_{PL} f_{2D}/1082 P^{1.156}\right)^{0.463 P^{0.0234}} - T_{b,IN} - q''_{PL} f_{2D}/h + T_{sat}}{q''_{PL} y_p / G C_p \pi d_t^2/4}. \tag{5}$$

If Z_{ONB} is larger than the length of the tube, L, the flow is entirely in the single phase regime. If Z_{ONB} is less than L, then the flow is in the single phase regime up to Z_{ONB}, and in the subcooled boiling regime from Z_{ONB} to L. The calculations of the pressure drop in these two regimes are described in the next two subsections.

Note that simplifying a complex heat transfer and flow situation using a corrected 1D approach provides a fast and convenient approach of understanding the situation through parametric analyses. However, it does involve approximations and, thus, carries uncertainties. For example, the extent of nucleate boiling along the circumference and length of the channel once ONB is reached would have a spatial 3D variation which is impossible to reproduce here. As an approximation, subcooled boiling is assumed uniform along the circumference of the channel and its inception is based on the scaled peak heat flux at the top of the channel. The results would then tend to overestimate the effect of subcooled boiling and to be conservative in this respect.

3.2.2. Single phase flow

For single phase flow, the pressure gradient, $(dP/dz)_{SP}$, depends on the coolant mass velocity, G, the density, ρ_f, the friction factor, f_f, and the coolant channel hydraulic diameter, d_t,

$$\left(\frac{dP}{dz}\right)_{SP} = \frac{-G^2 f_f}{2\rho_f d_t}. \tag{6}$$

In this equation f_f is the Fanning friction factor which can be estimated as a function of the flow Reynolds number, Re_f, and channel roughness, ε_r, based on Moody's expression (with 95% accuracy for Re_f between 4000 and 10^7 and ε_r/d_t of up to 0.01),

$$f_f = 0.0055\left[1 + \left(2\times 10^4 \frac{\varepsilon_r}{d_t} + \frac{10^6}{Re_f}\right)^{1/3}\right]. \tag{7}$$

The single phase pressure drop can be estimated by integrating Eq. (6) over the single phase length (Z_{ONB}, or L if the flow is entirely in the single phase regime).

3.2.3. Subcooled boiling flow

The pressure gradient in the subcooled boiling phase is more complex to analyse and depends on a number of additional factors such as the vapour bubble behaviour at the heated surface. Detailed physical modelling of these processes is lengthy and difficult without necessarily being very accurate. For simplicity and within the accuracy of the analysis presented here, the Owens and Schrock correlation was used [11]. The correlation was developed from sets of experimental data for water at pressures higher than atmospheric flowing in heated vertical tubes of length 0.4 m and diameter in the range 3–5 mm. For the limiter case considered, the ratio of length to diameter would be about the same but the actual length and diameter would be greater.

The correlation expresses the pressure gradient over the subcooled region normalised to the single-phase liquid pressure gradient at the same heat flux, velocity, and temperature, as a function of the water subcooling ratio between the end of the tube and Z_{ONB},

$$\frac{(dP/dz)_{SCB}}{(dP/dz)_{SP,equi}} = 0.97 + 0.28\exp(6.13Y), \tag{8}$$

$$Y = \left(1 - \frac{(T_{sat} - T_b)_{Z_{SCB}}}{(T_{sat} - T_b)_{Z_{ONB}}}\right). \tag{9}$$

The water bulk temperature can be calculated from the coolant inlet temperature and flow rate and from the heat flux in analogy to Eq. (4).

Eq. (8) can be integrated over the channel length where there is subcooled boiling (SCB), from Z_{ONB} to L (see Fig. 3) to estimate the total SCB pressure drop. Such an integration yields the following expression (assuming a constant $(dP/dz)_{SP,equi}$):

$$\Delta P_{SCB} = \left(\frac{dP}{dz}\right)_{SP,equi}\left(0.97(L - Z_{ONB}) + \frac{0.28}{C}\left(\exp(C(L - Z_{ONB}) - 1)\right)\right), \tag{10}$$

where C is

$$C = \frac{6.13 q''_{PL} y_p}{\left(GC_p \pi d_t^2/4\right)\left(T_{sat} - T_{b,in} - \left(q''_{PL} y_p Z_{ONB}/\left(GC_p \pi d_t^2/4\right)\right)\right)}. \tag{11}$$

The total pressure drop along the channel for the case where at least part of the flow is in the subcooled boiling regime can then be obtained by adding the integration of Eq. (6) over Z_{ONB} to Eq. (10).

3.2.4. Critical heat flux calculations

A large number of CHF correlations are available from the literature. However, most of these are for cases with uniform heat flux distributions. One of the uniform heat flux correlations that seems to provide reasonably good estimates for cases with parameters similar to the ITER PFC situation is the Tong-75 correlation [12]. Schlosser [13,14] conducted experiments on configurations and heat loads comparable to those of ITER PFCs. Based on his experimental results, he recommended using CHF_{uni} from the Tong-75 correlation scaled up by a factor of 1.2 in the case of regular tubes and 1.6 in the case of swirl-tape tubes (with twist ratio of 2) for estimating the peak heat flux on the tube under CHF conditions,

$$CHF_{uni}\,(W/m^2) = 0.23 f G h_{fg}\left(1 + 0.00216 P_{ratio}^{1.8}\,Re^{0.5}\,Ja\right), \tag{12}$$

$$P_{ratio} = \frac{P_{ex}}{P_c}, \tag{13}$$

$$Re = \frac{G d_h}{\mu_f}, \tag{14}$$

$$Ja = \frac{\rho_f}{\rho_g}\frac{C_p(T_{sat} - T)}{h_{fg}}, \tag{15}$$

$$f = 8\,Re^{-0.6}\left(\frac{d_h}{d_o}\right)^{0.32}, \tag{16}$$

where f is the friction factor calculated from Eq. (16), G is the mass velocity (kg/m^2 s), h_{fg} is the latent heat of vaporisation of water (J/kg), P_{ratio} is the ratio of exit pressure, P_{ex}, to critical pressure, P_c (= 22.1 MPa), Re is the Reynolds number, d_h is the hydraulic diameter (m), μ_f is the water viscosity (kg/m s), Ja is the Jakob number, ρ_f and ρ_g are the liquid and vapour densities respectively (kg/m^3), C_p is the water specific heat (J/kg K), T_{sat} is the saturation temperature (°C), T is the local temperature (°C) and d_o is a reference diameter = 12.7×10^{-3} m.

The above equations were added to RACLETTE. The ITER material and configuration choices can be simulated by two CHF scenarios. For the case with armour, Cu heat sink and Cu cooling channels, there is a resulting peak heat flux on the top of the cooling channel. In this case, to estimate the peak heat flux, CHF_{uni} from Eq. (12) is multiplied by the ratio 1.2 for regular tubes or 1.6 for swirl-tape tubes, as recommended by Schlosser [13,14]. Note that in this paper, consistent with the current design considerations, only regular tubes (without any CHF enhancement techniques) are assumed for the first wall region of the limiter, baffle and PFW modules.

The peak heat flux is scaled using a 2D focusing factor to estimate the corresponding 1D heat flux based on the pitch. To better evaluate this 2D focusing factor, 2D analyses were carried out using the F.E. ANSYS code [15] based on the geometry shown in Fig. 4. The ratio of peak coolant heat flux to incident heat flux depends on several factors such as the pitch to diameter ratio and the effective resistance of the cooling tube in series with the film convective heat transfer. The results are summarised in Fig. 4 for an ITER limiter pitch to diameter ratio of 2. For an incident heat flux of 5 MW/m^2 and a nominal coolant velocity of 7 m/s, both typical of the ITER limiter, the 2D focusing factor is 1.42 for a case without a SS insert in the channel. The 2D focusing factor is lower for the case with a SS insert as the larger thermal resistance of the SS results in larger heat diffusion around the circumference of the coolant channel. It varies between 1.3 and 1.15 for SS insert thicknesses of 0.1 and 0.3 mm respectively. For the purpose of the analysis, it was decided to use as a first order approximation an average 2D focusing factor of 1.3 ($\sim$ ratio of pitch to half channel circumference), and to determine the sensitivity of the results to changes in this factor.

3.3. Design parameters, material properties and heat loads

3.3.1. Design parameters

Table 1 lists typical design parameters and thermal loads anticipated for the ITER PFCs.

The maximum armour thickness is limited by the maximum allowable temperature under maximum steady-state design loads. Limits on the temperature arise from many concerns including melting, excessive vaporisation, reduced mechanical integrity, and chemical reactions during accidental exposure of armour or structure to air or steam. The latter limits are

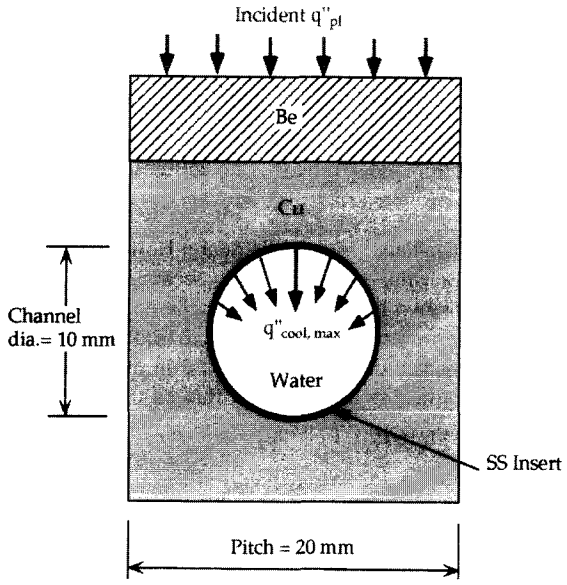

2-D focusing factor = Max. q''_{cool}/Incident q''_{pl}

Incident q''_{pl}	Eff. SS Insert Thickness	Finite Element 2-D Focusing Factor
5 MW/m^2	0 mm	1.42
5 MW/m^2	0.1 mm	1.3
	0.2 mm	1.23
	0.3 mm	1.15
> 10 MW/m^2	0 mm	>1.5

Fig. 4. Schematisation of the 2D focusing factor.

important particularly for carbon and beryllium for which explosion of hydrogen liberated from steam is a major concern. There is also a temperature-dependent limit for carbon self-sputtering due to radiation-enhanced sublimation. Tungsten, and tungsten-based alloys under consideration would produce radioactive products during neutron exposure that, at high temperature, might become volatile during a vacuum breach to air, and therefore be a risk for release. In particular, Rhenium, used to improve mechanical properties of W, is of particular concern because it becomes highly activated and adequate containment of the activated products would require extraordinary measures. The minimum armour thickness is based on preventing excessive heat fluxes through the armour/Cu interface to the coolant. Concerns include the effect of high thermal stresses at the interface and more importantly, for the limiter, the possibility of severe degradation of the coolant heat removal capability if CHF-like conditions are reached.

3.3.2. Material properties

The characteristic thermophysical material properties are summarised in Table 2, consistent with the ITER material database [16]. For CFCs, because of the high sensitivity of the thermal conductivity to n-irradiation, calculations were also performed using a reduced value of CFC thermal conductivity at 0.2 dpa obtained in R&D work by European researchers [17].

3.3.3. Surface heat loads

The term slow high-power transient often used in this paper refers to a type of plasma transient events whose duration is of the order of the characteristic thermal diffusivity time of a system which typically consists of a coolant tube embedded in a Cu-alloy heat sink structure on top of which is bonded the armour material. As an example, the characteristic time required

Table 1
Key design parameters and operation conditions used in the analysis

Design parameters/operating conditions	First-wall	Limiter	Baffle	Divertor
Coolant pressure (MPa)	~ 4.0	~ 4.0	~ 4.0	~ 4.0
Overall pressure drop under normal operation (MPa)	0.4–0.5	0.8–1.0	Inb: 0.4–0.5 Outb: 0.8–1.0	0.4
Inlet water temperature (K)	413	413	413	413
Coolant mass velocity (assumed) (kg/m^2 s)	2700	6300	2700	10000
Heat transfer coeff. (nominal) (kW /m^2 K) [a]	20	50	20	100–150 [b]
Coolant channel diameter (m)	1×10^{-3}	1×10^{-3}	1×10^{-3}	1.6×10^{-3}
Heat flux footprint length (m)	1 (assumed)	1 (assumed)	1 (assumed)	0.3
Pitch (m)	~ 2.2×10^{-2}	~ 2.0×10^{-2}	~ 2.0×10^{-2}	2.8×10^{-2}
Nominal/max. surf. heat flux (MW/m^2)	0.25/0.5	0.25/5	0.25/3	5
Max. energy density during transients (MJ/m^2)	60	60	60	
Transient duration (s)	≤ 0.3	≤ 0.3	≤ 0.3	≤ 10
Max. transient heat flux (MW/m^2)	200	200	200	≤ 30
Bulk heating (MW/m^3)	10–20	10–20	10–20	1–5
Armour material	Be	Be, CFC	Be (upper part)	Be, W, CFC
Armour thickness (mm)	~ 10 for Be	≤ 10 for Be	~ 10 for Be	≤ 10 for Be ≤ 20 for W ≤ 30 for CFC
Heat-sink material	Cu-alloy	Cu-alloy	Cu-alloy	Cu-alloy
Minimum heat-sink thickness (mm)	~ 2	~ 2	~ 2	~ 3
Coolant channel material	SS	Cu-alloy [c]	SS	Cu-alloy
Coolant channel thickness (mm)	1	1	0.5	3
Coolant channel roughness (μm)	50	50	50	50

[a] The correlation of Dittus–Boelter was used in the single phase regime, Thom's correlation was used in the fully developed subcooled boiling regime and a simple curve fit between the two (à la Bergles and Rohsenow) was applied in the transition region.
[b] Includes a turbulence promoter enhancement factor of ~ 1.9.
[c] With or without SS insert.

to conduct heat through a material slab 10 mm thick as a function of the temperature is shown in Fig. 5 for various materials. As an illustration of the range of thermal diffusion time constant, its value at 800 K is about 0.5, 0.7, 1, 2.5, and 10 s for non-irradiated CFC, DS-Cu, W, Be, and SS-316 LN respectively.

Table 2
Summary of main material properties used in the analysis (RT = room temperatures)

Key thermal properties		Beryllium [a]	Tungsten	C-fibre comp. [b]
Melting temperature, T_M	K	1556	3683 ± 20	3640 ± 25 [c]
Thermal conductivity, k (at RT)	W/m K	183	162	445 (< 100 [d])
Thermal conductivity, k (at T_M)	W/m K	60	83	< 100 (~ 100 [d])
Specific heat, C_p (at RT)	J/kg K	1760	132	440
Specific heat, C_p (at T_M)	J/kg K	3400	282	2300
Heat of fusion, h_{fg}	kJ/kg	1300	220	–
Heat of vaporisation, h_v	kJ/kg	36600	4800	59900 [e]
Emissivity, φ		0.61	0.4	0.75
Molecular weight		9	183.85	12
Parameters in sublimation rate equation [3]				
A_i	K	16720	44485	40181
B_i		11.61	12.74	14.80

[a] SB-65.
[b] Dunlop 3D P 120; for copper at RT, k = 350 W/m K, C_p = 385 J/kg K; for stainless-steel at RT, k = 14 W/m K, C_p = 471 J/kg K.
[c] Sublimation temperature.
[d] Refers to n-irradiated CFC (at ~ 0.2 dpa).
[e] This value assumes that mainly mono-atomic evaporation takes place. If instead, the formation of C_3 molecular carbon clusters is dominant a more appropriate value would be about 23000 kJ/kg.

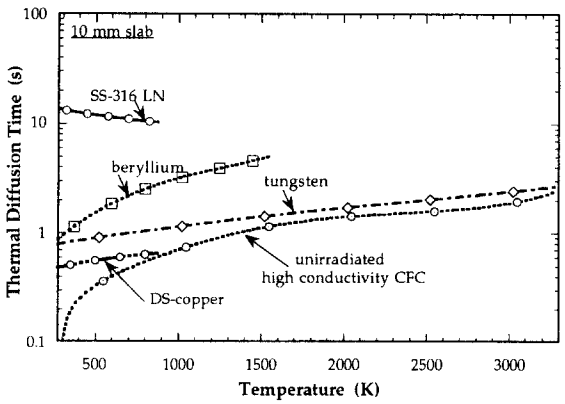

Fig. 5. Thermal diffusion time of various materials of interest (i.e., characteristic time required to conduct heat through a material slab) as a function of temperature assumed uniform through the bulk of a 10 mm thick slab. The thermal diffusion times scale as the square of the thickness.

3.3.3.1. Heat loads on limiter, primary first-wall and baffle. During the flat-top part of the burn the nominal heat flux on the ITER first wall is 0.25 MW/m^2. The maximum heat flux on the primary first wall is 0.5 MW/m^2 and on the baffle 3 MW/m^2. The limiter power loads, both at start-up and at plasma contact during burn, are dominated by alignment considerations. To avoid much higher heat loads at edges, the limiter segments have to be shaped so that the edges of the segment which is closest to the plasma are shadowed by the neighbouring segment [9]. During start-up and shutdown, the maximum design heat flux on the limiter is 5 MW/m^2. In addition, 'slow' high-energy deposition transients associated with plasma vertical displacement events (VDEs) can typically result in an energy density to the first wall armour of up to ~ 60 MJ/m^2 over ~ 0.3–1 s.

3.3.3.2. Heat loads on divertor plates. The present design of the ITER divertor is based on the so-called 'dynamic gas target regime' where a large fraction of the power incident on the scrape-off layer is already removed upstream by a combination of radiation and charge–exchange processes thus maintaining the heat flux to a level below about 5 MW/m^2. Slow transients can occur as off-normal events as the result of a transition from detached or partially detached divertor operation to fully attached operation. During these transients, the power increases above the maximum steady state design value of 5 MW/m^2. A peak value of 20 MW/m^2 and peak duration of 10 s is assumed here.

4. Results of the calculations

The thermal constraints for the limiter, baffle and primary first wall are first discussed, followed by a description of the detailed analyses performed for the more demanding limiter case. Finally, the analysis of the divertor plate is presented.

4.1. Thermal constraints on limiter, baffle and primary first wall

PFCs in ITER have to be designed to accommodate the maximum design heat flux under quasi steady-state. Thus, the armour and heat sink thicknesses are limited by the maximum acceptable armour temperature while the coolant parameters are set based on maintaining an acceptable critical heat flux and/or saturation margin. In addition, the limiter, primary first wall and upper portion of the baffle must be able to withstand off-normal heat loads resulting from plasma disruptions, and 'slow' high-energy deposition transients, such as those associated with plasma VDEs. In contrast to accommodation of steady-state high heat fluxes, accommodation of such high-energy deposition transients require thicker heat sink and armour regions to diffuse the energy to the coolant over a long time so that the maximum heat flux level is acceptable. Concerns arise from the high material temperatures and temperature gradients, in particular at the heat sink/armour interface where the material bonding could be affected, and from local coolant boiling. Local boiling is acceptable as long as it can be resorbed. However, the increase in flow resistance associated with two-phase flow can lead to flow starvation of the channel. If there is enough inertial energy in the first wall region, very high material temperatures could result. This could be analysed by assuming no heat flux to the coolant once critical heat flux conditions have been reached and determining the resulting material temperature histories.

4.1.1. Flow distribution following a VDE

A VDE could result in two-phase flow in the module first wall channels and in a substantial local increase in flow resistance. Such a scenario is more likely to lead to flow starvation in the case of parallel flow through the first wall and shield regions of the limiter and PFW modules, since the coolant would preferentially flow through the cooler lower-resistance shield region than through the higher flow resistance first wall. FW/shield series flow is preferable since it reduces the fraction of the total module flow path subject to two-phase flow increase in resistance. The effect of first wall two-phase flow must then be evaluated as part of the whole module pressure drop in comparison with other modules fed in parallel from the same manifold line but not subject to the VDE. (Note that a complete series flow through several modules is not possible because of the huge resulting pressure drop). Series flow through the first wall and shield region of high heat flux modules also provides for better flow distribution and a reduction in coolant flow rate. This occurs because the flow rate through the first wall region is based on maintaining acceptable critical heat flux margin and would be the same for either series or parallel flow scenarios. For the parallel flow case, an additional flow rate is required to cool the shield region.

Fig. 6 illustrates the general cooling system for ITER blanket modules. Three modules are shown as an example here but the cooling system could include additional modules. All modules are connected to the same inlet and outlet manifolds. For the limiter/outboard baffle cooling system of ITER, modules A and B would represent limiter modules while module C would represent the outboard baffle module.

The pressure drop through each module during normal operation is about the same if one assumes the pressure drop in the manifolds to be much smaller than the pressure drop through the modules. Through each module, the coolant flows in series through the first wall region and through the shield region as illustrated in module A in the figure. The desired flow rate though each module for the given pressure drop is set by using a flow control device, such as an orifice, where needed.

Following a VDE energy deposition in module A, for example, the heat flux to the coolant in the first wall region would increase and the local flow resistance would increase there also. The flow behaviour over the whole cooling system can be modelled by assuming that the total cooling system flow rate, m_{TOT}, is constant and by equalising the pressure drop, ΔP_i, through each module,

$$m_{TOT} = m_A + m_B + m_C, \tag{17}$$

$$\Delta P_A = \Delta P_B = \Delta P_C. \tag{18}$$

The pressure drop across modules B and C can be assumed to vary with the square of the mass flow rate through the respective module based on the single phase pressure drop expression.

$$\Delta P_i = \Delta P_{i,ini} \frac{m_i^2}{m_{i,ini}^2} \quad \text{for } i = B, C. \tag{19}$$

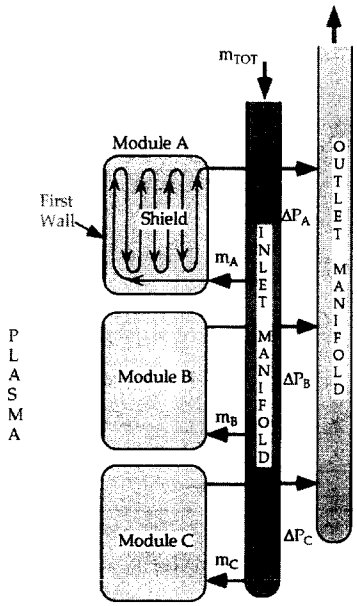

Fig. 6. Schematic of ITER blanket cooling system illustrating parallel flow through poloidally adjacent modules and series flow through the first wall and shield region of each module.

In addition, the pressure drop through module A can be divided in the pressure drop through the first wall region, $\Delta P_{A,FW}$, which is affected by the coolant heat flux situation and the heat flux through the shield, $\Delta P_{A,Sh}$. For simplicity, the pressure drop through the shield part of module A is also assumed to vary with the square of the mass flow rate through module A.

$$\Delta P_A = \Delta P_{A,FW} + \Delta P_{A,Sh,ini} \frac{m_A^2}{m_{A,ini}^2}. \tag{20}$$

For the flow resistance in the first wall region corresponding to a given coolant heat flux level, the mass flow rate through module A can then be obtained as follows. Expressions for ΔP_A, ΔP_B, and ΔP_C from Eqs. (19) and (20) can be substituted in Eq. (18), which can then be re-arranged based on the constant total mass flow rate assumption shown in Eq. (17), yielding

$$\Delta P_{A,FW} + \Delta P_{A,Sh,ini} \frac{m_A^2}{m_{A,ini}^2} = \Delta P_{i,ini} \left(\frac{m_{TOT} - m_A}{m_{TOT} - m_{A,ini}} \right)^2. \tag{21}$$

For a given $\Delta P_{A,FW}$ and given initial conditions, the corresponding mass flow rate, m_A, based on maintaining the same pressure drop through all the modules in parallel can be estimated by re-arranging Eq. (21) and solving for m_A.

Since the maximum design heat flux is higher for the limiter (5 MW/m^2) than for the baffle (3 MW/m^2) and PFW (0.5 MW/m^2), the thermal constraints on the limiter armour thickness are more severe. The limiter is thus chosen as the example case in the following section to show details of the analysis. The results for the baffle and primary first wall are then briefly presented at the end of the section.

4.2. Limiter analysis

4.2.1. Pressure drop under high coolant heat fluxes

The analysis proceeded by first estimating the pressure drop across the limiter first wall as a function of the mass velocity and the coolant heat flux based on the model described earlier. The flow regime was determined from the expression for Z_{ONB} (Eq. (5)) and the pressure drop was then calculated from Eqs. (6) and (10).

The results are summarised in Fig. 7 for a case assuming a coolant channel of diameter, pitch, length, and roughness of 0.01 m, 0.02 m, 1 m and 50 μm respectively. The coolant inlet temperature and pressure were assumed to be 413 K and 3.6 MPa, respectively.

For single phase flow, the pressure drop varies with the square of the mass velocity. This can be seen from the pressure drop variation at higher mass velocities and lower heat fluxes. For a heat flux of 5 MW/m^2, for example, fully single phase flow occurs for mass velocities above about 9800 kg/m^2 s. As the mass velocity is decreased below that value, the flow is partially in the subcooled boiling regime and the pressure drop diverges from the single phase variation. As the mass

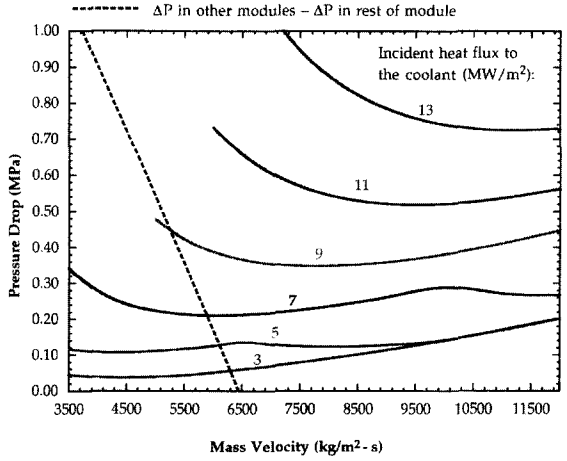

Fig. 7. Pressure drop across the limiter first wall region as a function of coolant mass velocity for different coolant heat flux levels (normalised to the pitch × length). Also shown is the relationship between the first wall pressure drop and mass velocity based on maintaining the same pressure drop across parallel modules for a fixed total coolant system mass flow rate.

velocity is decreased further to under about 6500 kg/m^2 s, the flow along the channel is completely in the subcooled regime and the pressure drop variation then shows a slight decrease with decreasing mass velocity followed by a sharp increase at lower mass velocity. This sharp increase is better illustrated by the higher heat flux cases.

On the same plot is shown the relationship between the first wall pressure drop and mass velocity based on maintaining the same pressure drop across parallel modules for a fixed total coolant system mass flow rate. This is based on Eq. (21). The total outboard baffle/limiter coolant system mass flow rate was assumed to be 3400 kg/s. Under normal conditions, the mass flow rate through a toroidal layer of limiter modules (e.g., module A in Fig. 6) would be 1460 kg/s with a total pressure drop of ~ 0.8 MPa, to which flow through 1 m of the first wall channel would contribute about 0.06 MPa.

For each heat flux level, the intersection of the first wall pressure drop curve with the curve derived from pressure drop equilibrium across parallel modules yields consistent values of first wall pressure drop and mass velocity. A set of such values is shown graphically in Fig. 8. These values for mass velocity and first wall pressure drop as a function of heat flux can then be used in RACLETTE. For simplicity, at each time step, the mass velocity and pressure at the end of the first wall are updated based on the heat flux to the coolant obtained at the previous time step. If more accuracy is required, an iterative procedure can be used to solve for the coolant heat flux and the mass velocity and pressure drop at the same time step, but it is quite cumbersome.

It is important to note that the assumption regarding the adjustment of coolant conditions based on the coolant heat flux at each time step in the calculations would be more valid for cases where the characteristic time for substantial heat flux to the coolant is much larger than the coolant residence time in a module. Typically, for the limiter, the coolant residence time is 0.2 s in the first wall and ~ 5 s for the whole module.

4.2.2. Limiter thermal response and coolant behaviour following a VDE

Several limiter cases were run using RACLETTE with the coupling of coolant conditions to the heat flux to determine the history of the heat flux to the coolant and the corresponding critical heat flux following a VDE. The VDE plasma energy density was set at 60 MJ/m^2 over 0.3 s after which the plasma is assumed to shutdown. It is not clear to what extent vapour shielding effects might mitigate the incident heat flux in the limiter case. As discussed in Refs. [3] and [7], vapour shielding would substantially reduce the amount of armour loss through evaporation and melting but would have a somewhat smaller effect on the heat flux seen by the coolant. To help ascertain its effect, cases assuming vapour shielding based on the simple model of Ref. [7] as well as cases assuming no vapour shielding were run. The CHF was evaluated as discussed in Section 3.2.4. The analysis was based on a limiter Cu-alloy channel (with and without a 0.2 mm SS insert) embedded in a Cu alloy heat sink block of thickness 2 cm with variable Be armour thickness. Other dimensions and parameters are consistent with those shown in Table 2.

To illustrate the findings, the results for a case assuming vapour shielding with no SS insert and a 6 mm Be armour are shown in Fig. 9(a). In this case the heat flux to the coolant reaches its maximum value within 1 s following the VDE since the rather high conductance of the thin Be armour and Cu-alloy heat sink results in lower inertial cooling effect. However, the heat flux to the coolant stays at a substantial level over the order of 10 s (not shown on the enlarged time scale of the figure). The coupling of the coolant conditions with the coolant heat flux is illustrated in Fig. 9(b) which shows the corresponding histories of the first wall pressure drop and outlet coolant temperature. Based on these evolving coolant

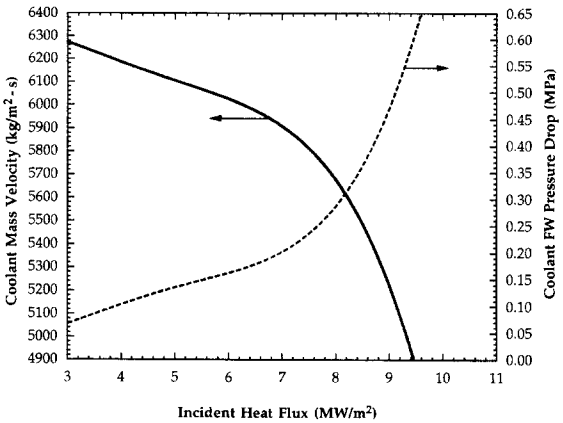

Fig. 8. Coolant mass velocity and first wall pressure drop as a function of incident heat flux for the limiter based on maintaining the same pressure drop across parallel modules.

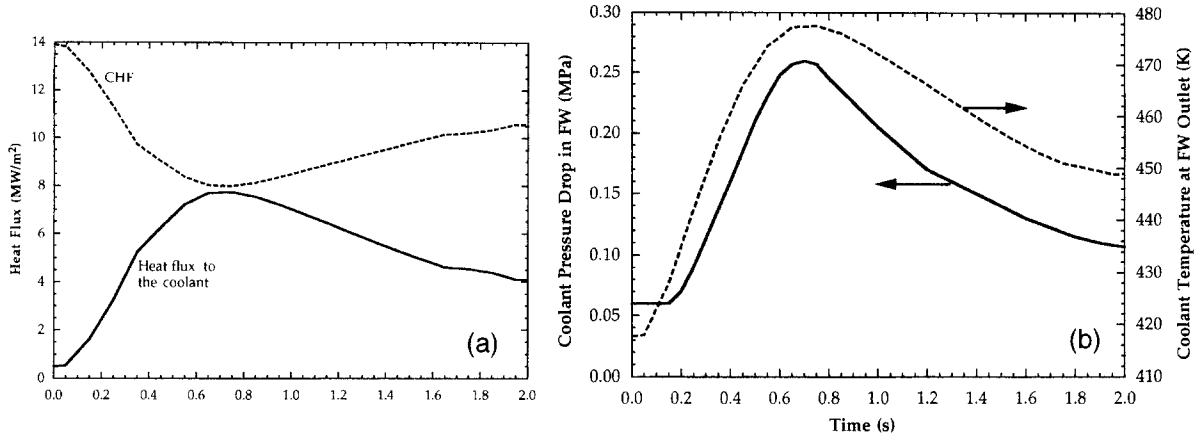

Fig. 9. (a) Histories of heat flux to the coolant and corresponding CHF following a 60 MJ/m^2, 0.3 s, VDE energy deposition for a case with 6 mm Be armour and vapour shielding. (b) Histories of coolant temperature at the outlet of the first wall channel and first wall channel pressure drop following a 60 MJ/m^2, 0.3 s, VDE energy deposition for a case with 6 mm Be armour and vapour shielding.

conditions including the mass velocity, the corresponding CHF (also shown in Fig. 9(a)) decreases from its initial value of ~ 14 MW/m^2 to a minimum value of about 8 MW/m^2. In this case, this lowest CHF value is still slightly higher than the corresponding coolant heat flux and the heat transfer process to the coolant is not interrupted.

As discussed in part I of this paper [3], for higher Be armour thicknesses, the inertial effect would increase, increasing the time over which the energy flows to the coolant but reducing the maximum heat flux to the coolant. This results in a wider margin between the maximum heat flux to the coolant and the corresponding CHF level. The reverse applies when the Be armour thickness is reduced. As an example, for a case with 5 mm Be armour, it was found that the heat flux to the coolant reaches the CHF after about 0.35 s when the CHF has dropped from its initial value of ~ 14 MW/m^2 to ~ 8 MW/m^2.

For this case, the corresponding temperature histories of the Be surface, Be/Cu interface and cooling channel are shown in Fig. 10. Since there is no surface heat flux anymore, following the assumed breakdown in heat transfer to the coolant once CHF conditions are reached, a thermal energy balance takes place resulting in a Be/Cu temperature of about 1073 K in this case. It is likely that such a temperature level would only last over the order of 1–10 s since, as the heat flux to the coolant is drastically reduced, coolant conditions would recover such as to provide at least some heat removal capability again. It is also possible that a full 3D analysis would reduce the resulting temperature level by better considering the cooler Cu mass behind the coolant tube. Thus, the question is whether the Cu/Be joint can accommodate temperatures of ~ 1000–1100 K over ~ 10 s when a VDE occurs. It is not clear yet what the preferred joining technique is. However, techniques such as brazing tend to be limited in the level of allowable temperature before bond softening and failure occur. It seems prudent at

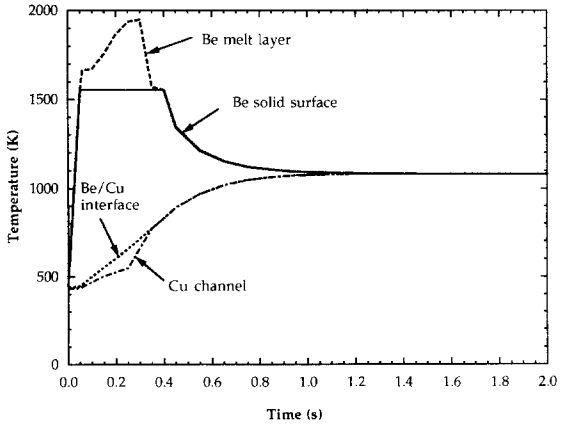

Fig. 10. Temperature histories of Be, Be/Cu interface and Cu channel following a VDE and a breakdown in the coolant heat removal capability.

this stage to design such as to completely avoid CHF-like conditions leading to severe degradation of heat removal capability. It is also important to note that an analytical assessment always carries some level of uncertainty stemming from both the analytical procedure and the assumptions used in the analysis. Thus, a parallel experimental effort is strongly needed to determine the consequences of such transients on the coolant conditions and on the Be/Cu joint integrity and to confirm the findings from the analytical assessment.

4.2.3. Limiter armour thickness

4.2.3.1. Be armour. Cases with different Be armour thicknesses were analysed using RACLETTE in a similar way as the example case described in the previous section. Fig. 11 summarises the results for cases with vapour shielding. It shows on the right-hand ordinate the ratio of coolant heat flux to CHF obtained from the analysis as a function of the Be thickness for cases with and without a 0.2 mm SS insert. In order to avoid severe degradation of the heat removal capability, the ratio of coolant heat flux to CHF should be less than unity. The corresponding minimum Be thickness should then be ~ 5.5–5.9 mm for cases with and without a SS insert for flow in a regular tube. Note that a somewhat lower thickness would be required in the case of a tube with swirl tape insert (lower by ~ 1 mm or less for a twist ratio of 2).

Also shown on the left-hand ordinate of the figure is the maximum Be temperature under maximum design heat load (5 MW/m^2 for the limiter) as a function of the Be thickness. It is not clear what is the maximum allowable temperature for Be. It tends to be a soft limit of ~ 900–1050 K based on degradation of the structural properties and on possible crack growth through the Be which could affect the Cu eventually. This limit needs to be better assessed through R&D. Assuming a limit of ~ 970 K, the maximum thickness of Be would then be ~ 6 and 7.3 mm for cases with and without a 0.2 mm SS insert. Changing this maximum temperature limit would affect the minimum Be thickness but by no more than ~ 1 or 2 mm in all likelihood.

In any case the Be thickness design window is small, ~ 5.5–6 mm and 5.9–7.3 mm for cases with and without a 0.2 mm SS insert respectively, and can be seriously affected by loss of armour due to erosion, vaporisation and perhaps more importantly loss of melt depending on the VDE frequency. The effective resistance between the surface and the coolant can affect the vaporisation loss and the melt thickness. However, in the range considered, both the Be armour thickness (3 to 10 mm) and the SS insert thickness (0 to 0.2 mm) have only a slight effect on the effective vaporisation loss and melt layer thickness, which in all cases are about 0.02 and 0.7 mm respectively. Of more concern is the assumption regarding the occurrence of mitigating vapour shielding effects. Cases run under the assumption of no vapour shielding indicate a melt layer thickness comparable to the above cases but a much higher evaporated thickness (~ 0.6 mm). The associated increase in the heat flux to the coolant also results in increasing the minimum Be required thickness by ~ 2.5 mm to prevent

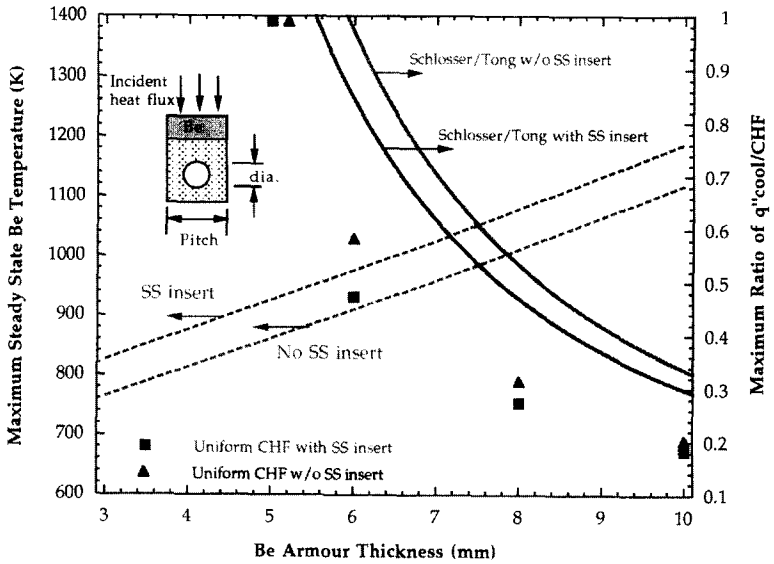

Fig. 11. Maximum Be armour temperature under maximum design heat load and ratio of coolant heat flux following a VDE (assuming vapour shielding) to CHF as a function of Be armour thickness.

CHF-like condtions following a VDE. Thus, in the absence of vapour shielding effects, the armour thickness design window can only be opened by increasing the maximum allowable Be temperature limit to ~ 1070 K or beyond.

For the basic performance phase of ITER, the anticipated number of VDEs is ~ 10–100. It is also planned to use a 'killer pellet' system to shutdown the plasma in case of a disruption such as a VDE. The efficiency and reliability of such a system will eventually determine the number of VDEs that the limiter will see. If it can be limited locally to one or two, the Be armour could be able to accommodate them even with loss of melt within the ~ 1 mm design margin. However, if the number of VDEs is significantly higher, loss of Be armour can result in failure at the Be/Cu bond due to degradation of coolant heat removal capability following a VDE. In this case, in situ repair measures such as plasma spray needs to be developed to ensure that Be armour can be used in the limiter.

It is worth mentioning that, in addition to vapour shielding, the major areas of uncertainty in these analyses include: 1) the plasma energy density that appears as heat on the PFCs armour; (2) the location of the incident area of the plasma energy; (3) the peaking factor of the plasma heat flux; and (4) the time over which plasma energy is deposited on the walls. The sensitivity of the results regarding several parameters was evaluated and are summarised below.

SS insert thickness: The effect has been reported as part of the discussion in the previous section. Basically, the SS insert increases the thermal resistance between the armour surface and the coolant resulting in an increase of the inertial cooling effect such that the energy diffusion to the coolant is spread over a longer time and the maximum coolant heat flux is reduced. The minimum Be thickness required for a case with a 0.2 mm SS insert is ~ 0.4 mm lower than for the case with no SS insert, as shown in Fig. 11. The effect on the maximum temperature limit is more marked, the corresponding maximum Be thickness for the case with no SS insert being higher by more than 1 mm than for the case without SS insert.

CHF calculations: As explained in Ref. [3], RACLETTE has been developed for a 1D geometry as a balance between reasonable accuracy for modelling a number of interrelated phenomena and ease and speed of computation. Approximating a 2D configuration with a 1D model using a 2D focusing factor for the CHF would always result in some uncertainty. To ascertain the effect of this assumption, cases were run where the heat flux was assumed to be uniformly distributed around the channel. The 2D focusing factor for the CHF calculations would then be the ratio of the pitch to channel circumference, about 50% of what was previously assumed in the calculations. The results are also shown in Fig. 11 (by the solid triangles and squares) for this uniform channel CHF case. Such a substantial change in the assumption would help but the effect is relatively small. The minimum required thickness decreases from 5.9 to 5.2 mm for the case without a SS insert and from 5.5 to 5 mm for the case with a 0.2 mm SS insert. Increasing the 2D focusing factor to 1.42 has a more marked effect, resulting in an increase in the required minimum Be thickness of ~ 1.5 mm. However, this might be too conservative since it does not take into account the redistribution of heat flux around the channel once CHF conditions are reached locally. If required, some additional margin could be obtained by using coolant tubes with CHF enhancement techniques, such as swirl tapes, albeit at the cost of higher pressure drop and manufacturing complexity. It must be noted that the coolant flow rates for the limiter as well as for the baffle and the primary first wall were set with the assigned objective of minimising the space and cost of the heat transport systems while maintaining acceptable thermal–hydraulic design margins under the maximum steady state design heat loads. Significantly increasing these flow rates would increase the CHF and help to some extent in decreasing the minimum Be armour thickness requirements but at the expense of bulkier, more expensive heat transport systems.

Channel roughness: The pressure drop calculations were done based on a limiter first wall channel roughness of 50 μm, conservatively allowing for possible roughening of the channel during operation due to fouling or other coolant/channel interactive processes. The same subcooled boiling flow analysis reported in Section 4.2.1 was carried out under the assumption of 10 μm roughness. Both the coolant mass velocity and FW pressure drop dependencies on the incident heat flux (see Fig. 8) are affected. The effect tends to be small at low incident heat fluxes but at higher incident heat fluxes ($> \sim 9$ MW/m^2), the resulting coolant mass velocity is higher by ~ 10% or more and the corresponding pressure drop in the FW channel lower by about 40% or more. However, when using these coolant mass velocity and pressure drop variations with incident heat flux as input in RACLETTE, values of the Be armour thickness at which the coolant heat flux equals the CHF are virtually unchanged from before (based on 50 μm roughness).

Time constants: The analysis assumes that the coolant residence time is smaller than the coolant heat flux time constant such that the coolant pressure drop and mass velocity can be adjusted at each time step assuming quasi steady-state conditions. Typically, for the first wall flow, this would be the case since the residence time is about 0.2 s for the limiter (and ~ 0.4 s for the primary first wall and baffle). However, for the whole module the residence time is of the order of 1–10 s. If the flow conditions were perturbed by the differential flow resistance between parallel first wall channels, the assumptions would be quite robust. However, the VDE energy deposition is assumed toroidally continuous over the row of poloidal first wall channels in each module. Thus, flow perturbation as assumed in the analysis is more likely to occur poloidally from module to module. In general, the analysis then tends to be quite conservative for cases with thinner armours where the coolant heat flux time constant is relatively short as, for example, for the 6 mm Be armour thickness shown in Fig. 9, where the maximum coolant heat flux occurs within 1 s and the heat flux stays at a substantial level over ~ 5–10 s. The

assumptions are more appropriate for cases with thicker armour thickness, as for example, for a case with 0.2 mm SS and 30 mm CFC armour. The maximum heat flux to the coolant then occurs at ~ 4 s and the coolant stays at a substantial level (about twice the initial value) over ~ 20 s.

A Be-armour case was also run assuming constant coolant mass velocity and pressure drop. For this case, only the coolant temperature at the outlet of the first wall channel is adjusted at each time step based on the coolant heat flux. This is reasonable since the coolant first wall residence time (~ 0.2 s or less depending on the footprint of the plasma heat flux) is smaller then the coolant heat flux time constant. It was found that the armour thickness at which CHF-like conditions were reached by the coolant differed only by a fraction of a mm. Of more importance then is the time constant required for the coolant to recover once CHF conditions are reached and the inertial coolant heat flux level starts decreasing. Such an assessment can only be determined experimentally with the relevant geometry and conditions.

Energy deposition characteristics: The results are dependent to varying level on the deposited energy characteristics, namely its density, deposition time and footprint. As discussed in Ref. [3], for the given energy density of 60 MJ/m^2, the heat flux to the coolant would increase with the energy deposition time up to a peak at an energy deposition time of the order of 1 s, depending on the PFC configuration. Thus, the coolant heat flux results shown here are conservative for deposition times shorter than 0.3 or much longer ones but not for deposition times between about 0.3 and 10 s. Typically, the melt layer thickness also peaks at a similar deposition time and then decreases quickly to zero at higher deposition time as the effective incident heat flux can be completely propagated through the armour by conduction. The effective evaporated armour thickness decreases with deposition time at an increasing rate down to zero within a deposition time of ~ 10 s. Once the energy density is high enough for Be melting to occur, the coolant heat transfer is not much affected by the assumed energy density level. Thus, the coolant heat flux results here are applicable to a rather large range of energy densities (~ 20 MJ/m^2–100 MJ/m^2 and probably higher). The major effect is on the amount of evaporated material and the melt layer thickness which both increase significantly with increasing energy densities. The assumed deposited energy footprint can certainly have a bigger effect on the results presented above since the amount of energy diffusing to the coolant is directly proportional to it. In this respect, the assumption of the full heat flux level to the coolant following a VDE falling on a 1 m channel length tends to be quite conservative and so are the results based on it.

Overall, the results are affected somewhat by the assumptions and choice of parameters. However, except for vapour shielding, the effect on the minimum Be thickness required to avoid severe degradation of coolant heat removal capability tends to be relatively small, within ~ ± 1 mm. Thus, the observations from the analysis are applicable within a rather broad range of assumptions and choice of parameters and tend to be quite robust in this sense. Within the uncertainties and assumptions, the minimum Be thickness required would then be in the range of ~ 5–7 mm and ~ 7–9 mm for cases with and without vapour shielding respectively, the upper values resulting in minimal or no design window depending on the maximum allowable Be temperature. This reinforces the observation that if the armour loss during operation is of the order of 1 mm, (e.g., for 1 VDE without vapour shielding or with significant loss of melt), in situ repair measures such as plasma spray following Be armour damages must be available for Be to be considered as limiter armour material.

4.2.3.2. CFC armour. Use of carbon fibre composite (CFC) armour as an alternative to Be was also investigated. Advantages of CFC include its rather high thermal conductivity and maximum operating temperature limit. The analysis used is the same as the one described previously for the case of Be. The geometry considered is also similar consisting of a CFC block in which runs a 1 mm thick, 10 mm diameter Cu coolant channel with or without a 0.2 mm SS insert. For the CFC material considered, the thermal conductivity degrades with irradiation decreasing sharply at first (within about 0.1 dpa) and at a lower rate as the radiation level is increased. For the analysis, the thermal conductivity at 0.2 dpa [17] is used corresponding to early operation during the basic performance phase of ITER.

CFC offers the possibility of a larger armour thickness design margin and the example results shown here conservatively assume no vapour shielding effects. Fig. 12 shows the CFC maximum temperature under the limiter maximum design heat flux (5 MW/m^2) and the ratio of coolant heat flux following a VDE to CHF as a function of the CFC armour thickness. As shown in the figure, a minimum CFC thickness of ~ 20 and 22 mm is required to avoid substantial degradation of heat removal capability of the coolant in the case of a Cu channel with and without a 0.2 mm SS insert, respectively. The material temperature consequences of such an event are comparable to the case of Be. Following a loss of coolant heat removal capability, the energy balance between the Cu channel and the CFC results in Cu and Cu/CFC interface temperatures of about 1073 K depending on the CFC thickness. Again, to avoid material degradation at the Cu/CFC interface, it is preferable that such a condition be avoided by design.

It is not clear what should be the maximum allowable CFC temperature under the maximum design load. It depends on different considerations such as radiation-enhanced sublimation which can result in unacceptably high plasma impurity levels, and safety concerns about carbon/water reaction at high temperature in case of accident [18]. Typically, maximum temperatures over the range 1500–1800 K have been considered. The corresponding maximum CFC thickness is about 27 to 39 mm depending on the maximum temperature assumed and on whether or not a 0.2 mm SS insert is used. No convincing

CFC in situ repair procedure has been proposed yet. Thus, as opposed to Be where plasma spray could be possible, the CFC has to rely exclusively on a sacrificial armour thickness. This sacrificial thickness ranges from about 5 to 19 mm depending on the assumed maximum allowable temperature limit and assuming a minimum thickness of 20–22 mm based on avoiding severe degradation of coolant heat removal capability, as discussed above. For the cases considered, the CFC evaporated thickness is about 0.2 mm per event. The available armour sacrificial thickness would then allow for ~ 25–95 such events assuming no other significant erosion mechanism. Note that if mitigating vapour shielding effects are assumed, the minimum required CFC thickness is reduced by several mm's and evaporation following a VDE is drastically reduced. The combination of these two effects result in substantially extending the CFC armour lifetime.

Thus, based on this analysis, CFC provides advantages over Be in accommodating VDEs and maximum temperature limits, and it is considered as an alternate limiter armour material. The major concerns which must be addressed in using CFC is the high chemical erosion rate which can result in high tritium inventory through codeposition on the cooler nearby surfaces and in the divertor, and the higher baking temperature required for surface conditioning of the limiter following venting or a major disruption.

4.3. Primary first wall and baffle analysis

The limiter is subject to higher heat loads than the primary first wall and baffle, which results in a more restrictive armour thickness design window for the limiter. Thus, the analysis and discussion presented above have focused on the more challenging limiter case. Here, implications of VDE transient energy deposition on the primary first wall and top part of the baffle in combination with maximum allowable steady state armour temperature limits are summarised. The lower part of the baffle represents a different situation and is not considered here. It is subject to much higher neutral sputtering erosion which governs the choice and thickness of armour material.

For both the baffle and primary first wall case, the coolant mass velocity is ~ 2700 kg/m^2 based on maintaining reasonable CHF margin under maximum design heat flux and margin to saturation under power excursion respectively. An analysis of the coolant heat flux following a VDE was done for this case also. The minimum Be thickness to avoid severe degradation of coolant heat removal capability was found to be ~ 8 and 10 mm for cases with and without vapour shielding. For the primary first wall case, the maximum design load is 0.5 MW/m^2 and the Be armour thickness can be of several centimetres based on maintaining the maximum Be temperature ~ 900–1000 K. The maximum thickness in this case would be based on Be block manufacturing and bonding technique and thermo-mechanical performance during operation. A Be armour thickness of > ~ 12–15 mm would provide a reasonable margin particularly if plasma spray in situ repair is possible. For the baffle, the constraint is more severe since the maximum heat load is 3 MW/m^2. A Be armour thickness of ~ 10 mm would result in a maximum Be temperature of ~ 950–1000 K for a Cu tube with a 0.5 mm SS insert. This would provide a rather small armour design window which could be increased by relaxing the maximum allowable Be temperature.

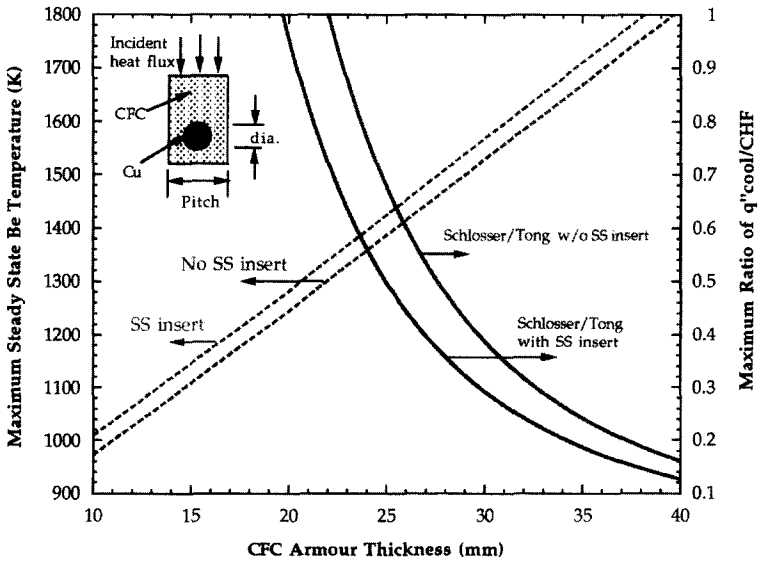

Fig. 12. Maximum CFC armour temperature under maximum design heat load and ratio of coolant heat flux following a VDE (assuming no vapour shielding) to CHF as a function of CFC armour thickness.

The situation is slightly better than that of the limiter but only a very limiter number of VDEs could be accommodated by the upper part of the baffle unless in situ Be armour repair measures are taken (e.g., plasma spray).

4.4. Divertor

This section presents the results of several analyses conducted to evaluate the thermal and material responses during power transients of actively cooled divertor plates consisting of an armour bonded to a heat sink substrate. Several cases have been investigated for the three different candidate materials presently considered for the protection of divertor PFCs (i.e., Be, W, and CFC) to understand the effect of various design/operation parameters, such as the plasma heat flux to the surface, the armour thickness, and the duration of the transients, and of material behaviour, such as the possibility of vapour shielding, the fraction of melt layer loss for metal armours, and neutron effect on properties (e.g., in degrading the thermal conductivity of C-based armours,). The results of these analyses are important and have strong implications on the design of the ITER divertor PFCs as they contribute to defining the choice of the most adequate clad materials and of their thicknesses. Some discussion on this subject has been presented in Ref. [19].

The dimensioning of the divertor plates is determined primarily by the heat loads under steady-state operating conditions which is assumed here to be ~ 5 MW/m^2. The design of these plates, however, has to accommodate unavoidable high-recycling transients burning through the gas target regime near the strike points which will last up to a few seconds and increase substantially the surface heat-flux to about 10–30 MW/m^2. Concerns arise from the high material temperatures and temperature gradients, in particular at the heat sink/armour interface where the material bonding could be affected. As for the limiter, the accommodation of such high-power deposition transients requires thicker armours. The incident heat flux could be attenuated to some extent by low density vapour shielding effects. These may arise as armour vaporisation increases with the surface temperature, leading to a conversion of some of the incident power to plasma radiation, a fraction of which continues to fall on the plate, reaching about 25% of the incident power.

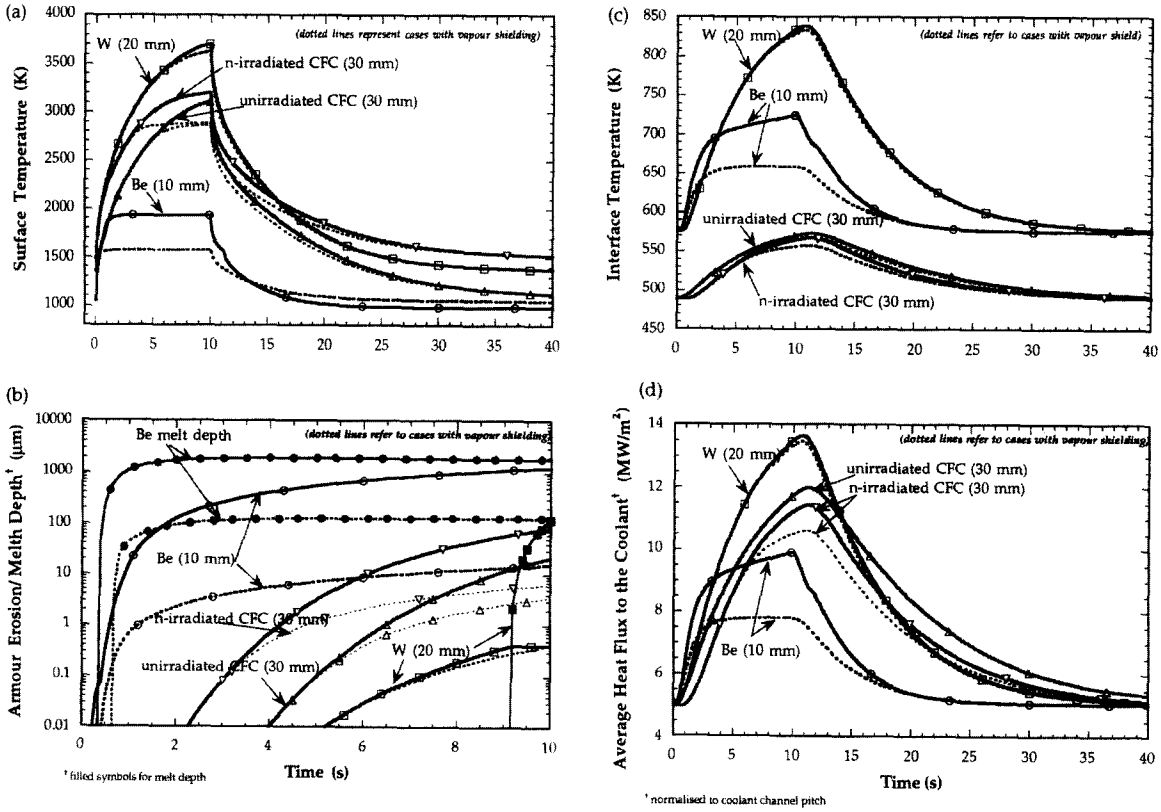

Fig. 13. (a) Surface temperature as a function of time for a power transient of 20 MW/m^2 lasting 10 s, (dotted lines refer to cases with vapour shielding). Assumed armour thicknesses are: 10 mm Be, 20 mm W and 30 mm CFC. (b) Corresponding armour erosion (vaporisation only) and melt layer depth as a function of time. (c) Corresponding armoury/heat-sink interface temperature as a function of time (dotted lines refer to cases with vapour shielding). (d) Corresponding heat flux to the coolant (normalised to coolant channel pitch) as a function of time.

Note that, in contrast to the limiter case, the possibility of severe degradation of coolant heat removal capability based on CHF-like conditions is not a major issue for the divertor cases considered. For these cases, the CHF tends to be significantly higher than the coolant heat flux following high heat flux transients due to a number of considerations including:

1. The maximum transient heat flux level is lower and the assumed duration of these events longer than for the limiter case. The footprint of such events in the divertor case is also assumed lower than in the limiter case by a factor of ~ 2. These result in diffusion of the energy to the coolant over a shorter length and over a longer time with a lower maximum coolant heat flux.
2. The coolant mass velocity for the divertor is higher than that for the limiter by about 50% and it is planned to use a swirl tape in the higher heat flux region of the divertor channel to enhance heat transfer, the combination of which results in CHF in the divertor being higher than the limiter case by about a factor of 2 or more.
3. High heat flux events are assumed toroidally uniform in the divertor region. Thus, the increase in flow resistance in the affected region is similar for the different divertor cassettes being fed in parallel. Consequently, there is no redistribution of the flow based on differential flow resistance that could result in flow starvation of one cassette.
4. It is believed that vapour shielding mechanisms resulting in incident heat flux attenuation is more likely in the divertor region than in the limiter region based on the time constant for dissipation of the vapour cloud.

4.4.1. Histories of temperature, heat flux, melted and evaporated thickness for different materials

At first, an analysis was conducted to better understand the effects of these thermal transients on PFC structures similar to those shown in Fig. 2. For the different plasma facing materials, the time evolution of important parameters was determined, including the temperatures at the armour surface and at the armour/heat sink interface, heat flux to the coolant, thickness vaporised and depth of the melt layer (for metals) during the transient. The armour thicknesses assumed for this analysis were: 10 mm for Be, 20 mm for W and 30 mm for CFCs and the parameters and material properties are those summarised in Tables 1 and 2. A sudden power transient from 5 MW/m^2 to 20 MW/m^2 lasting 10 s was assumed for the calculations.

Fig. 13(a) shows the armour surface temperature history, and the corresponding histories of ablated and melt layer

Table 3
Summary of results of calculations done by varying the power flux at constant armour thickness (10 mm Be, 20 mm W, 30 mm CFC) [a]

Parameters	Beryllium		Tungsten		CFC [b]	
	with VS	w/o VS	w VS	w/o VS	w VS	w/o VS
5 MW/m^2						
$T_{X,max}$ (K)	1054	1054	1370	1370	1020 (1495)	1020 (1495)
$T_{I,max}$ (K)	575	575	575	575	490 (488)	490 (488)
$q''_{coolmax}$ (MW/m^2) [c]	5	5	5	5	5 (4.95)	5 (4.95)
δ_{evap} (μm)	~ 0	~ 0	~ 0	~ 0	~ 0	~ 0
δ_m (μm)	~ 0	~ 0	~ 0	~ 0		
10 MW/m^2						
$T_{X,max}$ (K)	1515	1745	2273	2273	1755 (2223)	1755 (2223)
$T_{I,max}$ (K)	650	680	680	681	532 (523)	532 (523)
$q''_{coolmax}$ (MW/m^2) [c]	7.5	8.5	8.5	9.4	8.5 (7.72)	8.5 (7.72)
δ_{evap} (μm)	~ 5	80	~ 0	~ 0	~ 0 (~ 0)	~ 0 (~ 0)
δ_m (μm)	~ 0	1230	~ 0	~ 0	–	–
20 MW/m^2						
$T_{X,max}$ (K)	1572	1930	3629	3703	2855 (2885)	3054 (3199)
$T_{I,max}$ (K)	659	725	829	834	578 (557)	581 (565)
$q''_{coolmax}$ (MW/m^2) [c]	7.8	9.91	13.3	13.5	12.6 (10.6)	12.8 (11.3)
δ_{evap} (μm)	15	1250	~ 0	~ 0	3 (7)	12 (85)
δ_m (μm)	165	1830	~ 0	~ 115	–	–
30 MW/m^2						
$T_{X,max}$ (K)	1590	1995	3830	4520	2930 (2938)	3341 (3366)
$T_{I,max}$ (K)	660	765	868	930	585 (561)	596 (575)
$q''_{coolmax}$ (MW/m^2) [c]	7.9	11.2	14.6	16.7	13.1(10.9)	14.3(12.2)
δ_{evap} (μm)	21	2560	5	145	~ 13 (16)	~ 460 (675)
δ_m (μm)	255	1760	1050	3740	–	–

[a] Results include cases with and without vapour shielding (VS), and for CFC n-irradiation effects on thermal conductivity (~ 0.2 dpa).
[b] Values in parentheses refer to n-irradiated CFC (at 0.2 dpa).
[c] Normalised to channel pitch.

thicknesses (for metal, assuming no melt layer loss) during the power transient are shown in Fig. 13(b). Both cases with and without vapour shielding are shown in the figures. From these two figures, it can be seen that, for Be, the surface temperature rapidly exceeds the melting temperature of the material (T_m = 1556 K), and the melt depth, when vapour shielding is not included, and assuming no loss mechanisms, is about ~ 1830 μm at the end of the transient and the erosion due to evaporation is about 1250 μm. Vapour shielding reduces dramatically both the evaporated (~ 15 μm/event) and the melt layer thickness (~ 165 μm/event). At the end of the transient, the surface temperature drops sharply and the PFC cools at a rate which is determined by the thermo-physical properties of the armour and heat sink materials and the coolant parameters. The melt resolidification time (not shown within the time scale of Fig. 13(b)) is roughly the same as the duration of the transient (10 s). For a 20 mm thick tungsten tile, the surface temperature increases up to the maximum value of about 3700 K and in the absence of vapour shielding effects melting takes place only marginally (~ 115 μm) during a fraction of the last second of the transient. Loss of material is only due to vaporisation and is negligible at the end of the transient (less than 1 μm). For a 30 mm thick CFC tile the maximum temperature reached is ~ 3050 K for the case of unirradiated material and ~ 3200 K for n-irradiated CFC. For the case with vapour shielding the maximum temperature remains below ~ 2900 K for both cases with and without vapour shielding. The corresponding loss of material due to evaporation amounts to 85 μm for n-irradiated CFC (10 μm for the case with vapour shielding) and just few μm's for the case with vapour shielding as shown in Fig. 13(b).

Fig. 13(c) shows the armour/heat sink interface temperature history for the same thermal transient and Fig. 13(d) shows the corresponding history of the heat flux to the coolant normalised to the coolant channel pitch. The peak temperature at the interface and the peak heat flux to the coolant are highest for the case with a W tile 20 mm thick (~ 835 K and ~ 13.5 MW/m^2, respectively) as most of the heat onto the plate will be removed by conduction to the coolant and evaporation and black-body radiation are still very low for the surface temperature indicated in Fig. 13(a). For Be, the maximum temperature at the interface with Cu-alloy heat sink is ~ 725 K and ~ 660 K, respectively, for the case with and without vapour shielding. The corresponding heat flux to the coolant is ~ 10 MW/m^2 and ~ 8 MW/m^2, respectively. This can be taken as indicative of the thermal stress at the armour/Cu joint, whose heat flux limit needs to be evaluated experimentally for the relevant geometry and conditions. Finally, for a CFC monobloc, the solution peak temperature at the interface with Cu tube is lowest (< 570 K) and the peak heat flux to the coolant varies between 10.5–12.8 MW/m^2.

To better evaluate the effects of varying the peak surface heat flux on the parameters calculated and plotted in Fig. 13(a) to (d), analyses were conducted for the different armour materials with the same thicknesses as above (i.e., 10 mm thick Be tile, 20 mm thick W tile and 30 mm thick CFC tile), and the results are summarised in Table 3. Cases with and without vapour shielding are shown. The depth of the melt which develops for the metals has been obtained assuming that there is no loss of the melt layer during the power transient. For CFCs, results are also reported including effects of reduced thermal conductivity induced by modest n-irradiation (~ 0.2 dpa).

From the results of the calculations summarised in Table 3, it is seen that negligible evaporation takes place below about 5–10 MW/m^2 for Be and about 15–20 MW/m^2 for W and CFC for the case without vapour shielding. Vapour shielding reduces dramatically the evaporation at higher fluxes (e.g., from 1250 μm to 15 μm for Be, negligible evaporation for W, from 12 μm to 3 μm for unirradiated CFC, for a surface heat flux of 20 MW/m^2). For 10 mm Be and 20 mm W, melting is negligible below surface heat fluxes of about 5 MW/m^2 and 20 MW/m^2, respectively. Vapour shielding reduces the melt layer thickness at higher fluxes (e.g., for a plasma heat flux of 20 MW/m^2, the melt layer is reduced from 1830 to 165 μm for Be, and from 115 to ~ 0 μm for W). For CFC, for a given heat flux, the main effect resulting from the degradation of the thermal conductivity due to n-irradiation is the increase of the peak surface temperature at the end of the transient (e.g., ~ 3200/3050 K and ~ 2885/2855 K for a 20 MW/m^2 surface heat flux for n-irradiated/non-irradiated CFC, for cases without and with vapour shielding, respectively). The evaporation heat loss and the armour erosion are then higher (e.g., 85/12 μm and 7/3 μm for n-irradiated/non-irradiated CFC, for a heat flux of 20 MW/m^2 without and with vapour shielding, respectively). The heat conducted through the plate to the coolant is always higher for the case without vapour shielding as the thermal gradient across the armour tile is higher.

4.4.2. *Effect of varying the armour thickness*

Hereafter are described the results of a study to evaluate the effect of varying the thickness of the armour for the different armour materials. The thickness of the armour material is a key parameter which needs to be specified for the design of the PFCs in ITER. For a given power level, it determines the temperature and stress distribution during normal operation and their change with time during transients. From the design performance standpoint, lower temperatures at the armour/heat sink interface are required to minimise the differential expansion and stress due to the mismatch of the coefficients of thermal expansion. Also, thermal gradients across the armour have to be minimised as they induce large stress. The reduction of the armour thickness due to a combination of various mechanisms (e.g., sputtering, evaporation during disruptions and other slower thermal events, and for metals, possible loss of melt) has also to be taken into account in the design process.

For the design of the ITER divertor PFCs, the armour thickness upper limit is based primarily on the maximum allowable surface temperature for steady state operation at the maximum design heat load (5 MW/m^2), and its lower limit is based on the maximum heat flux across the armour/heat sink interface to the coolant as well as by the peak temperature at the interface during the transients of interest here. The temperature limit on a PFC design will be driven primarily by thermal stresses and degradation of structural properties in the armour and at the armour/heat-sink joint. These depend strongly on the design solution to be adopted on the basis of ongoing R&D results (e.g., 'stress-free' PFC concepts such as castellation, brush-type armour, use of compliant thermal contact layers, functionally graded armour/heat sink joints, etc.) [20]. In addtion, manufacturing considerations must also be taken into account in setting the maximum armour thickness. For the example divertor analysis presented here, beginning-of-life (BOL) thicknesses of about 10, 20 and 30 mm are considered reasonable for Be, W and CFC, respectively. The corresponding maximum steady state temperatures are ~ 1050 K, ~ 1400 K and ~ 1500 K for Be, W and 0.2 dpa CFC, respectively, which, for the latter two materials, tend to be conservative.

For Be, the peak heat flux to the coolant normalised to the pitch (as indicative of the armour/Cu interface thermal stress), the interface temperatures, and the maximum steady-state temperature are plotted as a function of the thickness in Fig. 14(a), and the resulting armour erosion per shot is plotted in Fig. 14(b). Erosion of the armour here comprises vaporisation and loss of melt. Two cases of continuous loss-of-melt are shown, corresponding to 10% and 50% loss of the incremental melt layer calculated at each time step in the analysis.

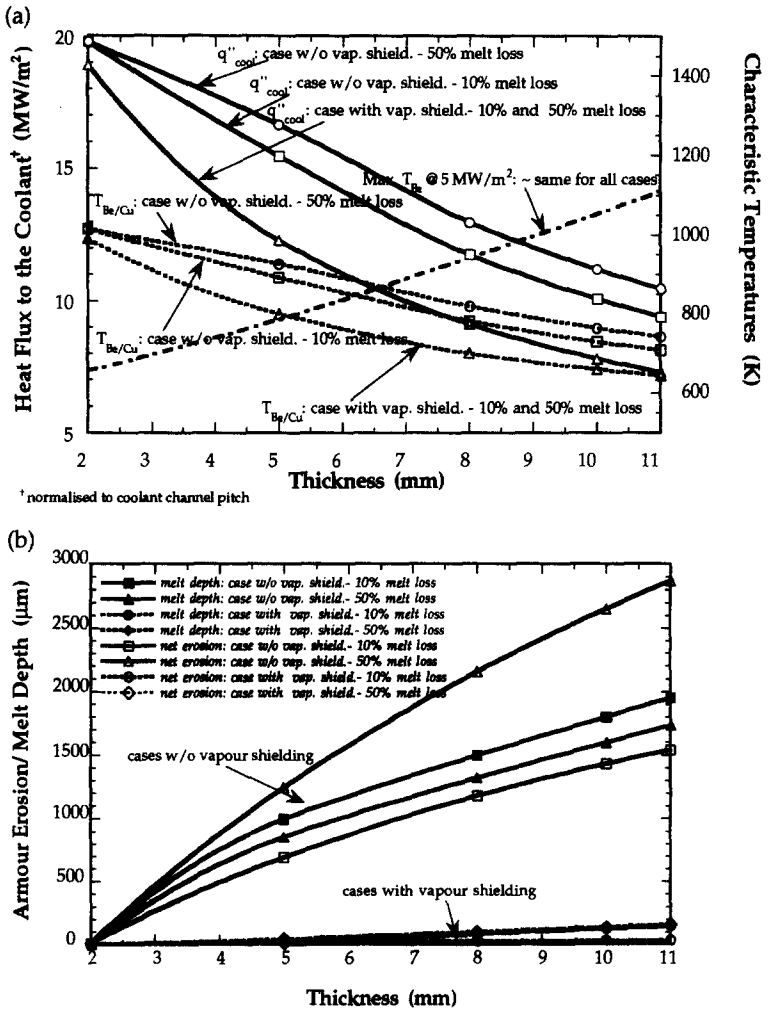

Fig. 14. (a) Heat flux to the coolant (normalised to the coolant channel pitch), and temperatures at the armour/heat-sink interface as a function of the target thickness for Be for a power transient of 20 MW/m^2 lasting 10 s, assuming no vapour shielding. Also, indicated on the figure, is the variation of the surface temperature as a function of the armour thickness for a steady-state nominal heat flux of 5 MW/m^2. (b) Erosion depth (vaporisation and partial loss of melt for two cases 10% and 50%, respectively).

For W similar plots are shown in Fig. 15(a) and (b). As for Be, erosion here comprises vaporisation and loss of melt. Two cases of continuous loss-of-melt are shown, corresponding to 10% and 50% loss.

For CFC, Fig. 16(a) shows the peak heat flux to the coolant and the peak value of the temperature during the transient as a function of the armour thickness, while Fig. 16(b) plots the resulting armour erosion which, contrary to the case with metals, is only due to vaporisation. Cases including n-irradiation effects are also shown.

From the results of the above calculations, it is clear that the thinner the armour material, the lower the peak surface temperature and erosion at the end of the transient, but the higher the armour/interface peak temperature and the peak heat flux to the coolant. Design criteria such as fixing the maximum allowable temperature at the braze joint and the maximum heat flux through the PFC block to the coolant would set limitations on the maximum tolerable sacrificial thickness (i.e., thickness to be eroded from the beginning of life of the component to its end of life (EOL)). Unfortunately, at the present time, it is not quite yet possible to set for the different materials a unique set of such maximum values. Results from on-going R&D would shed some light in this respect and are eagerly awaited.

For instance, if one assumes a maximum heat flux through the armour/Cu interface and to the coolant of ~ 15 MW/m^2 (e.g., to prevent armour debonding due to excessive thermal stresses) an EOL Be armour thickness of 5.5–6.5 mm would be acceptable for the case with no vapour shielding and 3.5 mm for the case with vapour shielding. For tungsten and CFC,

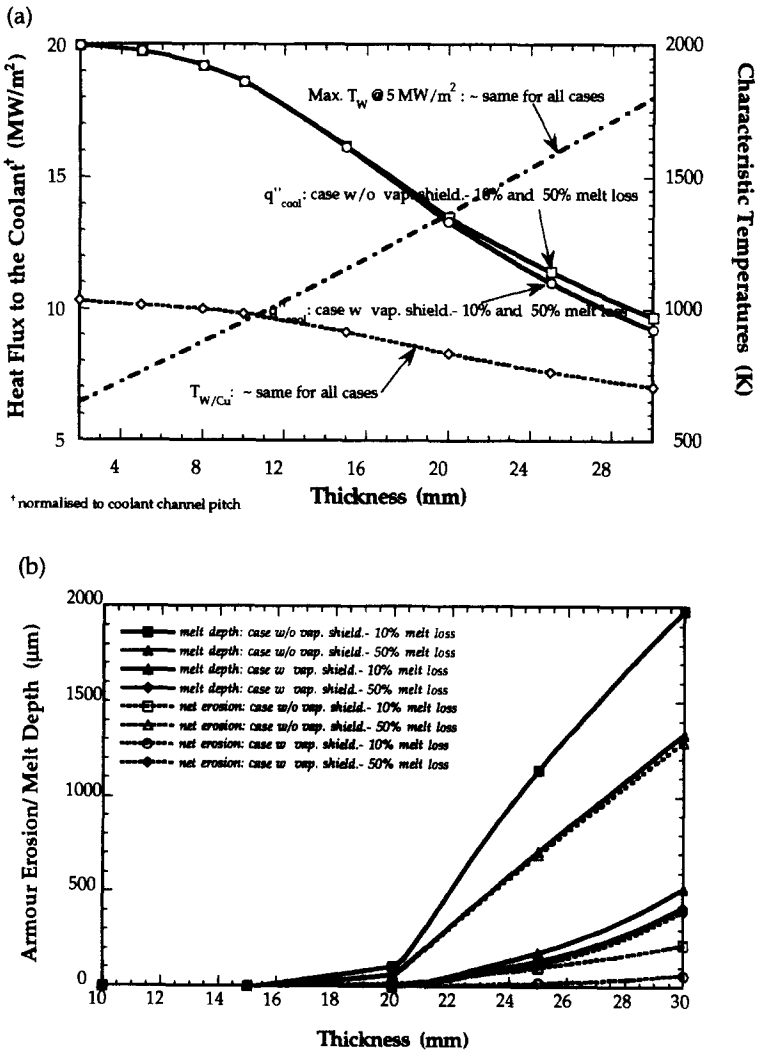

Fig. 15. (a) Heat flux to the coolant (normalised to the coolant channel pitch), and temperatures at the armour/heat-sink interface as a function of the target thickness for W for a power transient of 20 MW/m^2 lasting 10 s, assuming no vapour shielding. Also, indicated on the figure, is the variation of the surface temperature as a function of the armour thickness for a steady-state nominal heat flux of 5 MW/m^2. (b) Erosion depth (vaporisation and partial loss of melt for two cases 10% a nd 50%, respectively).

results are less sensitive to vapour shielding and ~ 17 mm of W and ~ 25 mm of CFC (~ 20 mm considering n-effects) would be accepted as EOL thickness. The sacrificial depth would then be ~ 6.5 mm (~ 3.5–4.5 mm w/o vapour shielding), ~ 3 mm, and ~ 5–10 mm for Be, W and CFC with assumed BOL thicknesses of 10, 20 and 30 mm respectively. These numbers are quoted as examples only since the ongoing R&D will determine the joining technique. The joint constraint depends on the design (e.g., a CFC monobloc will have less stringent constraints) and should result from 3D analysis of temperatures and stresses, and the maximum allowable heat flux to the coolant may be higher, depending on design of the cooling system. If one assumes that a very robust joining technique can be developed and that the peak heat fluxes can be handled by the cooling system, one could accept to go down to much lower minimum thickness and then the sacrificial thicknesses would be much increased (for example for a 2 mm thick armour at the EOL, sacrificial thickness would be ~ 8 mm for Be, ~ 18 mm for W, and ~ 18 mm for CFC).

4.4.3. Armour erosion induced only by slow transients

In addition to the heat transfer aspects associated with transient events a strong bearing on the design and lifetime arises from the exact amount of vaporisation loss of the melt layer per event and its accumulation with the number of events. To this aim a study was conducted for the three materials, including and excluding vapour shielding effects, to evaluate the rate of reduction of the armour thickness due to thermal transients only, considering partial loss of melt and for CFCs reduction of the thermal conductivity due to n-effects. As it has already been shown, during power excursions on the divertor plates,

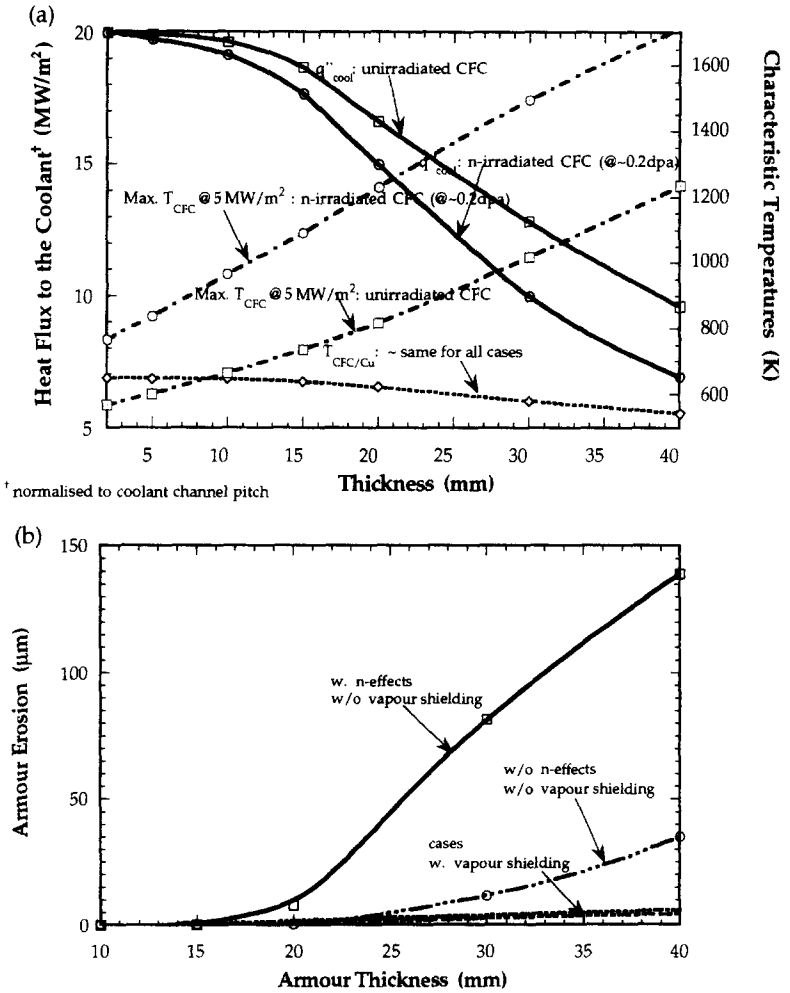

Fig. 16. (a) Heat flux to the coolant (normalised to the coolant channel pitch), and temperatures at the armour/heat-sink interface as a function of the target thickness for CFC for a power transient of 20 MW/m^2 lasting 10 s, assuming no vapour shielding. Also, indicated on the figure, is the variation of the surface temperature as a function of the armour thickness for a steady-state nominal heat flux of 5 MW/m^2. (b) Erosion depth (vaporisation) for unirradiated and n-irradiated (~ 0.2 dpa) CFC as a function of the armour thickness.

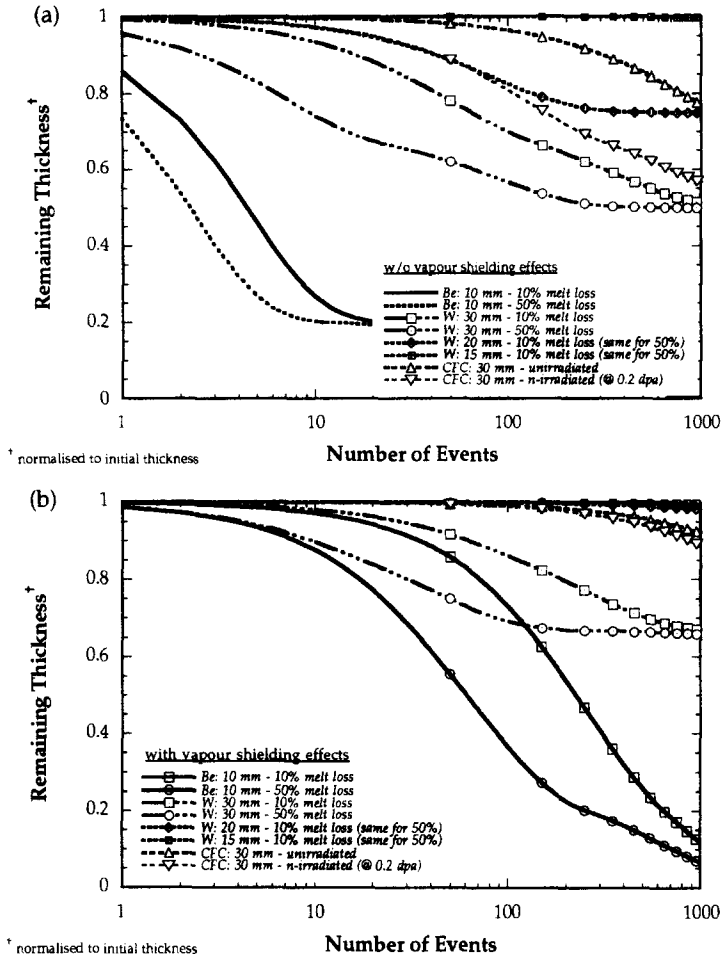

Fig. 17. Reduction of armour thickness (normalised to initial thickness) as a function of number of transients events. Cases considered were: 10 mm Be tile, 15, 20 and 30 mm W tiles, 30 mm CFC tile. For the metals two cases are shown with 10% and 50% loss of melt, respectively. For CFC both unirradiated and n-irradiated CFC (at ~ 0.2 dpa) were considered. (a) Cases without vapour shielding; (b) cases with vapour shielding.

the net erosion is caused by both evaporation and loss of the melt layer, and depends strongly on the surface temperature and therefore on the remaining thickness at the time of the shot. The results are summarised in Fig. 17(a) and (b) which show the remaining armour thickness as a function of the number of transient events excluding and including vapour shielding effects, respectively. In light of thsee results, for the case of Be, only a few events (< 10) may be sufficient to reduce the thickness of the armour to an unacceptable design level if vapour shielding plays no or only a marginal role. Vapour shielding would substantially extend the number of shots up to a few hundreds. The situation is much improved for W and CFC where, even in the absence of vapour shielding effects, on the order of a thousand such events may be withstood.

These results are only indicative since only erosion resulting from slow high-power transients is considered. For the interested reader, more extended discussions on the evaluation of the composite erosion lifetime of divertor plate armour resulting from (1) the slow transients considered here, (2) disruption erosion and (3) sputter erosion in normal operation are given in Refs. [20–23]. However, the trends of the different materials is clear, as is the importance of the various parameters considered (e.g., vapour shielding effects, fraction of melt loss, initial thickness).

5. Conclusions

This paper presents the results of a design assessment study conducted to evaluate the thermal and material response of PFCs in the ITER device subject to 'slow' high power thermal transients. The analyses were performed by using the RACLETTE Model, described in part I of this paper. The model has been recently developed to provide a flexible design

tool to predict heat transfer and erosion of duplex-structured PFCs, under plasma deposition transient whose duration is comparable or longer than the characteristic thermal diffusion time of the component. It accounts for multi-regime heat-transfer evaluation at the coolant side based on the evolving coolant conditions and for change-of phase of the armour material. Evaporation, melting, thermal radiation, conduction and convective heat transfer to the coolant are considered in determining the armour thermal response. An improvement of the computational capabilities of the original model is described in this paper. It is particularly applicable to the limiter case. It includes a methodology to evaluate the critical heat flux, the change of the coolant parameters and the severe degradation of coolant heat removal capability that could result under certain conditions during these transients. Vapour shielding effects as calculated from a simplified model [7] have been included for some calculations.

Cases were chosen to provide detailed analytical results for the relevant ITER PFC configurations, materials, conditions and combination of phenomena. Armour materials considered include Be for the primary first wall and upper baffle region, Be and CFC for the limiter, and Be, CFC and W for the divertor. Results for ITER PFC cases have been presented and discussed, including armour sizing analyses. These are helping the ongoing design assessment conducted to select adequate plasma protection materials and optimise the design of ITER PFCs. Based on these results, the following general observations can be made:

- 'Slow' high power transients result in high armour and heat sink temperatures, higher heat flux to the coolant, and severe surface erosion of the tile because of vaporisation and, for metals, partial loss of the melt layer. The magnitudes of these resulting effects depend heavily on the occurrence of mitigating vapour shielding effects that have been recently speculated by Igitkhanov et al. [7], but not fully demonstrated by experiments [10]. In this regard, the scarcity of experimental data is evident and effort should be directed to this area in order to better assess the effectiveness (if any) of such a phenomenon in reducing transient peak heat fluxes in the different ITER PFC regions, as this would markedly impact the PFC armour lifetime and design choices. A careful planning and evaluation of tokamak experiments to investigate the formation of low-density vapour shield in a tokamak plasma is required.
- The thermal constraints on the armour thickness were identified for the cases of the limiter, first wall, baffle and divertor. The maximum armour thickness is limited by the maximum allowable temperature under maximum design loads. This tends to be a soft limit for Be, CFC, and W and needs to be more precisely defined through experiments. The minimum armour thickness is based on preventing excessive heat fluxes through the armour/Cu interface to the coolant. Concerns include the effect of high thermal stresses at the interface and, more importantly for the limiter, the possibility of severe degradation of the coolant heat removal capability if CHF-like conditions are reached following a VDE.
- For the Be limiter case, the minimum armour thickness required to prevent CHF-like conditions in the coolant and the resulting high Be/Cu interface temperature following a VDE was estimated. The resulting Be thickness design window is small and depends on the maximum allowable steady-state temperature assumed for Be ($\sim$ 5.9–7.3 mm for a case without a SS insert assuming vapour shielding and a maximum Be temperature limit of $\sim$ 970 K). The absence of vapour shielding would increase the minimum Be thickness requirement by $\sim$ 2.5 mm. In this case, the armour thickness design window can only be opened by relaxing the maximum allowable Be temperature to $\sim$ 1070 K or more. This window can also be seriously affected by loss of armour due to erosion, and more importantly vaporisation ($\sim$ 0.6 mm per VDE in the case of no vapour shielding) and loss of melt ($\sim$ 0.7 mm per VDE) depending on the VDE frequency. For the basic performance phase of ITER, the anticipated number of VDEs is $\sim$ 10–100. If it can be limited to one or two by means of some emergency plasma shutdown measure (e.g., killer pellet), the Be armour could be able to accommodate them within the $\sim$ 1 or 2 mm design margin. However, if the number of VDEs is significantly higher, loss of Be armour can result in failure at the Be/Cu bond due to degradation of coolant heat removal capability following a VDE. In this case, in situ repair measures such as plasma spray needs to be developed to ensure that Be armour can be used in the limiter.
- For the CFC limiter case, the minimum thickness required is about 20–22 mm to avoid CHF-like conditions in the absence of vapour shielding. The sacrificial thickness ranges from about 5 to 19 mm depending on the assumed maximum allowable temperature limit. For the cases considered, the CFC evaporated thickness is about 0.2 mm per event. The available armour sacrificial thickness would then allow for $\sim$ 25–95 such events assuming no other significant erosion mechanism. Vapour shielding would reduce the minimum thickness requirement by several millimetres and drastically reduce the evaporation per VDE, resulting in a much longer lifetime. Thus, based on this analysis, CFC provides advantages over Be in accommodating VDEs and maximum temperature limits in particular if the number of VDEs is more than one or two and if remote in situ plasma spray repair for Be is not feasible. CFC concerns which must be addressed include the redeposition process which can result in high tritium inventory through codeposition processes taking place on the cooler CFC surfaces and the higher baking temperature requirement for limiter surface conditioning.
- For the baffle and primary first wall, the coolant mass velocity is about half that of the limiter. The minimum Be thickness to avoid severe degradation of coolant heat removal capability was found to be $\sim$ 8 and 9.5 mm for cases with and without vapour shielding. For the primary first wall case, the maximum design load is 0.5 MW/m^2 and the Be

armour thickness can be of several cms based on maintaining the maximum Be temperature ~900–1000 K. The maximum thickness in this case would be based on Be block manufacturing and bonding technique and thermo-mechanical performance during operation. For the baffle, the constraint is more severe since the maximum heat load is 3 MW/m^2. For a case with a 0.5 mm SS insert in the Cu coolant channel the armour design margin is rather small (~ 1 or 2 mm). A more comfortable margin could be achieved by increasing the maximum allowable Be temperature and/or reducing the SS insert thickness. The situation is slightly better than that of the limiter but only a very limited number of VDEs could be accommodated by the upper part of the baffle unless in situ Be armour repair measures are taken (e.g., plasma spray).

- For the divertor 'vertical target' region under a power transient from 5 MW/m^2 to 20 MW/m^2 over 10 s, Be armour appears to be inadequate for protecting the PFC in the absence of vapour shielding effects because of the large resulting erosion per transient (vaporisation and loss of the melt) and the low resulting lifetime. The erosion lifetime of the divertor plate will be determined by the frequency of these transients and the combination of other synergistic erosion processes like sputtering and disruptions, whose effects are of particular concern for the Be exposed to divertor load conditions.
- For the W divertor case, even without vapour shielding, melting does not occur below 20 mm and erosion due to vaporisation is small. However, concern remains for the resulting high temperature at the armour/heat sink interface and high heat flux to the coolant during every transient. Debonding of the armour and minimisation of the thermal stresses associated with the thermal gradient in the armour, may require special advanced armour solutions, such as brush and functionally graded W/Cu layers [20] and need to be analysed.
- CFC monobloc-type solution seems to perform best for the divertor as erosion (due to vaporisation only) and peak armour/heat sink temperature are moderate.
- In addition to 'slow' high power transient effects, the composition of other events, including sputtering and disruptions, will ultimately determine the erosion lifetime for the different armour materials. Of particular concern is the partial or total loss of the melt layer for metals, resulting from disruptions, and the high chemical sputtering rates for CFC.
- Vapour shielding plays a key role in substantially reducing vaporisation and melting (up to an order of magnitude) and in extending the divertor armour lifetime. Based on the divertor results with vapour shielding and on the sacrificial depths estimated from the analysis, the numbers of high-power transients that could be tolerated before repair are about 200 for Be, and a very large number (> 1000) for W and for CFC.

Finally, it should be noted that the results of the analyses presented here carry uncertainties arising both from the model approximations [3] and the uncertainties of the material properties, and, more importantly, from the limited experimental data available for model calibration. Thus, these results should be regarded as: providing a general guide to the magnitudes and trends associated with different mechanisms and phenomena, including evaporation and melting, and vapour shielding; identifying areas of concerns such as the coolant behaviour during a VDE; and providing approximate design window for certain parameters, such as the armour thickness. As new results become available and improvements are made, the modelling analysis will be updated. In the end, however, only experimental results can completely validate the choice of PFC armour and a strong experimental effort is required in this area.

6. Nomenclature

C parameter defined in Eq. (11);

C_p specific heat of the material;

CHF critical heat flux;

d_t coolant channel diameter;

d_h hydraulic diameter;

d_o reference diameter used in calculating f in Eq. (16);

f friction factor defined in Eq. (16);

f_f Fanning friction factor;

f_{2D} geometry factor to account for 2D effects;

G coolant mass velocity;

h convective heat transfer coefficient;

h_{fg} latent heat of vaporisation of water;

Ja Jakob number;

k material themal conductivity;

L channel length;

m coolant mass flow rate;

Nu Nusselt number;

P pressure;

P_{ratio} ratio of exit pressure to critical pressure;

Pr Prandtl number;

q'' heat flux;

q''_{ONB} coolant heat flux at Onset of Nucleate Boiling;

q''_{pl} plasma heat flux;

Re Reynolds number;

T temperature;

T_A surface temperature of armour;

T_b coolant bulk temperature;

T_I armour/heat-sink interface temperature;

y_p coolant channel pitch;

Y parameter defined in Eq. (9);

z distance coordinate along coolant tube length;

Z_{ONB} coolant tube length over which the flow is entirely in the single-phase regime.

6.1. Greek symbols

δ_{evap} effective evaporated thickness;

δ_m melt layer thickness;

ΔP pressure drop;

ε_r channel roughness;

μ water viscosity;

ρ material density.

6.2. Subscripts

b bulk;

c critical;

cool coolant;

evap evaporation;

equi equivalent;

ex exit;

f film;

FW first wall;

IN inlet;

ini initial;

max maximum;

ONB Onset of nucleate boiling;

pl plasma;

sat saturation;

SCB subcooled boiling;

Sh shield region;

SP single phase;

uni uniform;

w wall.

Acknowledgements

The authors had several useful discussions with Drs H.D. Pacher and I. Smid of the European ITER Home Team, which they wish to acknowledge also for their technical input and suggestions. They are also grateful to Mrs Birgit Esser for her help with the computer programming and to Dr S. Chiocchio for his review of the manuscript and his helpful suggestions. This report was prepared as an account of work performed under the Agreement among the European Atomic Energy Community, the Government of Japan, the Government of the Russian Federation, and the Government of the United States

of America on Co-operation in the Engineering Design Activities for the International Thermonuclear Experimental Reactor ('ITER EDA Agreement') under the auspices of the International Atomic Energy Agency (IAEA).

References

[1] Y. Igitkhanov, G. Janeschitz, H.D. Pacher and M. Sugihara, in: Proc. 22nd EPS Conf. Contr. Fusion/Plasma Physics, Bournemouth, UK, July 1995, IV: 317–320.
[2] G. Janeschitz, K. Borrass, G. Federici, Y. Igitkhanov, A. Kukushkin, H.D. Pacher, G.W. Pacher and M. Sugihara, J. Nucl. Mater. 220–222 (1995) 73.
[3] A.R. Raffray and G. Federici, this issue, p. 85.
[4] G. Janeschitz, Plasma Phys. Control. Fusion 37 (1995) A19.
[5] K. Ioki and Members of the ITER JCT and Home Teams Blanket Group, ITER Blanket System Design, 19th Symposium on Fusion Nuclear Technology, Lisbon, Sept. 1996, to be presented.
[6] E. Tada, K. Ioki, G. Janeschitz, D. Maisonnier and E. Martin, in: Proc. 16th Symp. on Fusion Engineering (SOFE), Champaign-Urbana, Vol. 1, Oct. 1995, p. 399.
[7] Y. Igitkhanov, H.D. Pacher, G. Federici, G. Janeschitz, D.E. Post and I. Smid, in: Proc. 22nd EPS Conf. Contr. Fusion/Plasma Physics, Bournemouth, UK, July 1995, IV: 453–456.
[8] D.E. Post, B. Braams, J. Mandrekas, W. Stacey and N. Putvinskaya, in: Proc. 5th Int. Conf. on Plasma Edge Theory, Monterey, CA, Dec. 4–6, 1995, contrib. to Plasma Phys., to appear.
[9] Technical Basis for the ITER Interim Design Report, Cost Review and Safety Analysis, ITER EDA Doc. Ser. No. 7, IAEA, Vienna (1996).
[10] J.D. Tubbing, A. Chanking, S. Clement, P. Coad, E. Deksnis, J. Lingertat, A. Loarte and C. Lowry, in: Proc. 22nd EPS Conf. Contr. Fusion/Plasma Physics, Bournemouth, UK, July 1995, III: 453–456.
[11] J.G. Collier, Convective Boiling and Condensation, 2nd Ed. (McGraw-Hill, New York, 1982).
[12] L.S. Tong, Proc. AIChE-ASME 1975 Heat Transfer Conf., ASME Publ., 75-HT-68, 1976.
[13] J. Schlosser and J. Boscary, Final Report, PDT 2–4 Task, STID, Association EURATOM-CEA, Cadarache, France, Mar. 31, 1994.
[14] J. Schlosser, private communication (May 1995).
[15] ANSYS User's Manual for Revision 5.1, Swanson Analysis Systems, Inc. Houston, PA, USA, Sept. 1994
[16] ITER Material Database, in preparation.
[17] C.H. Wu et al., J. Nucl. Mater. 212–215 (1994) 416.
[18] R.E. Nygren and M.F. Smith, Fusion Technol. 19 (1991) 2092.
[19] G. Federici, A.R. Raffray, H.D. Pacher, I. Smid, S. Chiocchio, B. Esser, J. Dietz, Y. Igitkhanov and G. Janeschitz, in: Proc. 16th Symp. on Fusion Engineering (SOFE), Champaign-Urbana, Oct. 1995, Vol. 1, p. 430.
[20] R. Matera, G. Federici et al., J. Nucl. Mater. 233–237 (1996) 17.
[21] ITER Interim Design Report, Section 1.7 Appendix E, July 1995.
[22] H.D. Pacher, I. Smid and G. Vieider, NET Internal Note N/I/3330/17/B, Sept. 1995.
[23] H.D. Pacher, I. Smid, G. Federici, Yu. Igitkhanov, G. Janeschitz, R. Raffray and G. Vieider, in; Proc. 12th Int. Conf. on Plamsa Surface Interactions in Controlled Fusion Devices, 20–24 May, 1996, St. Raphael, France, J. Nucl. Mater. (1997) in press.